



**DURABILITY OF MWCNT COMPOSITES UNDER ELECTRON AND  
NEUTRON IRRADIATION**

THESIS

Quan Hai T. Lu, Major, USA

AFIT/NUCL/ENP/12-M05

**DEPARTMENT OF THE AIR FORCE  
AIR UNIVERSITY**

**AIR FORCE INSTITUTE OF TECHNOLOGY**

---

---

**Wright-Patterson Air Force Base, Ohio**

DISTRIBUTION STATEMENT A  
APPROVED FOR PUBLIC RELEASE; DISTRIBUTION UNLIMITED

The views expressed in this thesis are those of the author and do not reflect the official policy or position of the United States Air Force, Department of Defense, or the United States Government. This material is declared a work of the U.S. Government and is not subject to copyright protection in the United States.

AFIT/NUCL/ENP/12-M05

DURABILITY OF MWCNT COMPOSITES UNDER ELECTRON AND  
NEUTRON IRRADIATION

THESIS

Presented to the Faculty

Department of Engineering Physics

Graduate School of Engineering and Management

Air Force Institute of Technology

Air University

Air Education and Training Command

In Partial Fulfillment of the Requirements for the  
Degree of Master of Science in Nuclear Engineering

Quan Hai T. Lu, BS

Major, USA

March 2012

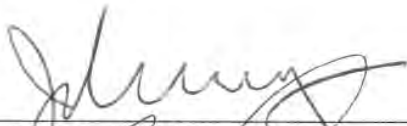
DISTRIBUTION STATEMENT A  
APPROVED FOR PUBLIC RELEASE; DISTRIBUTION UNLIMITED

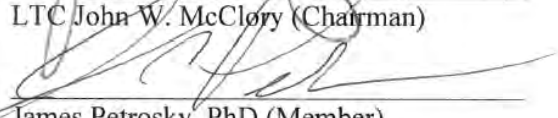
DURABILITY OF MWCNT COMPOSITES UNDER ELECTRON AND  
NEUTRON IRRADIATION

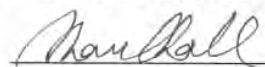
Quan Hai T. Lu, BS

Major, USA

Approved:

  
\_\_\_\_\_  
LTC John W. McClory (Chairman)

  
\_\_\_\_\_  
James Petrosky, PhD (Member)

  
\_\_\_\_\_  
Shankar Mall, PhD (Member)

7 MAR 12  
Date

06 Mar 12  
Date

03/06/2012  
Date

### **Abstract**

Electromagnetic interference shielding effectiveness and conductive properties of carbon nanotube containing composites intended for use as satellite surface materials have been investigated following electron and neutron irradiation. The multi-walled carbon nanotube (MWCNT) composites have low resistivity that is consistent with conductive materials. Two sets of MWCNT composites have been assessed. One set was used to investigate electron irradiation effects and the other neutron irradiation effects. Each panel consisted of four plies of MWCNT infused on epoxy resin and four plies of space grade SiO<sub>2</sub> glass in different layered configurations. One panel, consisting of eight plies of SiO<sub>2</sub> glass and no MWCNTs served as the control sample.

The MWCNT composites were irradiated to fluence levels of  $10^{16}$  electrons/cm<sup>2</sup> with 500 keV electrons. Increase in EMI-SE and conductivity was observed following electron irradiation in two of the samples. The sample with alternating layers of MWCNT and glass had a decrease in conductivity and an increase in EMI-SE post irradiation. This would suggest that the different layered configuration does play a role in the durability of the composite. Having multiple conductive layers of MWCNT composites provide increased durability against electron irradiation. Additionally, changes in conductivity are not the only mechanism affecting the EMI-SE of the composite. Additional electron irradiations were conducted on three MWCNT composite with the two layers of MWCNT on the outside and 4 layers of glass sandwich in the center. The panels were irradiated to a fluence of  $10^{16}$  electrons/cm<sup>2</sup> with 100, 200, and

500 keV electrons to investigate the possibility of ionizing effects on the MWCNT composite. However, no changes in the EMI-SE were observed for these irradiations. The second set of MWCNT composites were irradiated with 1.0 MeV Si(eq) neutrons to a fluence level of  $10^{14}$  neutrons/cm<sup>2</sup> and  $10^{15}$  neutrons/cm<sup>2</sup>. Minor changes in the conductivity and no change in EMI-SE was observed in the MWCNT composites. The overall changes observed; however, are inconsequential to MWCNT composites' intended use as satellite surface structure.

In addition, the different layered configurations did have an effect on the electrical properties and durability of the composite under irradiation. The sample with the alternating layer of MWCNT and glass had the least favorable configuration of the three designs. Initial EMI-SE was lower than the other two layered configuration and a greater decrease in conductivity was observed post irradiation. The configuration with the two layers of MWCNT on the outside had the best design. The design allows the composite to shield against both external and internal sources of EMI. In addition, it was the design that had the least changes to its electrical property post electron and neutron irradiation.

## Table of Contents

	Page
Abstract .....	iv
Table of Contents .....	vi
List of Figures .....	viii
List of Table .....	xi
List of Symbols and Acronyms .....	xii
I. Introduction .....	1
1.1 Objective of Research .....	2
1.2 Paper Organization .....	3
II. Characterizing the Problem .....	5
2.1 The Space Environment .....	5
2.2 Space Vehicle Charging .....	7
III. The Material .....	9
3.1 Carbon Nanotubes .....	10
3.2 Epoxy Resin Polymer .....	12
3.3 Composite Material .....	13
3.4 Electrical Conductivity of MWCNT .....	14
3.5 Conductivity of MWCNT composites .....	15
3.6 Gas Absorption/Desorption Model of MWCNT Composites .....	17
IV. Model for Radiation Effects .....	20
4.1 Neutron Non-Ionizing Energy Loss .....	21
4.2 Electron Irradiation .....	22
4.3 Radiation Effects on MWCNT Composites .....	24
4.4 Radiation Effects on Epoxy Resin .....	25
4.5 Radiation Effects on Carbon Nanotube .....	26
4.6 Summary .....	29
V. Experimental Procedure .....	31
5.1 Experiment Overview .....	31
5.2 Description of the Tested Material .....	31
5.3 Resistivity Measurements .....	33
5.4 Thermoelectric EMFs Compensation Methods .....	40
5.5 Resistivity of Bulk Materials (Volume Resistivity) .....	41
5.6 Experimental Set-Up .....	42

5.7	Resistivity Measurement Procedure.....	42
5.8	EMI Shielding Effectiveness Theory .....	47
5.9	Measurement Technique .....	51
5.10	EMI-SE Measurement Procedure .....	53
VI.	Sample Irradiation .....	55
6.1	Overview .....	55
6.2	Dynamitron Electron Irradiation .....	56
6.3	Neutron Irradiation .....	58
VII.	Results and Analysis .....	61
7.1	CASINO <sup>®</sup> Simulation Results.....	61
7.2	Pre-characterization Results and Analysis .....	64
7.3	Post Vacuum Result and Analysis .....	69
7.4	Electron Irradiation Results.....	71
7.5	Electron Irradiation Analysis .....	73
7.6	Neutron Irradiation results .....	78
7.7	Error Analysis .....	80
VIII.	Conclusion and Recommendation .....	84
	Appendix A.....	88
	Bibliography .....	89



## List of Figures

Figure	Page
1. Van Allen Inner and Outer Belt [5] .	5
2. 90 wt% Multi-walled Carbon Nanotube Bucky Paper [8].	9
3. SWCNT and MWCNT [9].	10
4. Hybrid $sp^2$ -orbitals of carbon atoms forming a hexagonal network. [11] .	11
5. The rolling of a graphene sheet determines the three types of CNT [32].	12
6. Simple model of electron flow in material. ....	14
7. Percolation level of MWCNT composites [14].	16
8. Plot of DC conductivity of two types of MWCNT composite as a function of MWCNT content. ....	17
9. Gas Absorption/Desorption Model [17].	18
10. Radiation induced damage in MWCNT and CNT bundles [23].	26
11. Irradiation gives rise to current redistribution damaged [23].	28
12. Stacking Configuration of MWCNT Composites.....	32
13. The four point probe method (left) and method of images (right) [35] .	35
14. The Two Wire Resistance measurement [40].	38
15. The Four-Wire Resistance Measurements [40].	39
16. The Four-Wire Resistance Measurements [40].	42
17. Bulk resistivity measurement setup. Keithley 4200 SCS on the left and	43
18. 1 Resistivity test fixture used to mount samples.....	44
19. Copper samples used to verify surface conductivity measurements. ....	46
20. Electromagnetic wave propagating through a solid conductive material [6].	48

Figure	Page
21. Multiple internal reflections.....	49
22. Network Analyzer used to measure EMI-SE.....	52
23. Sample holder for EMI-SE measurement. ....	53
24. Samples mounted on the cold head. Sample for EMI-SE on the left .....	57
25. Ohio State University Research reactor. ....	60
26. Results of CASINO <sup>®</sup> simulation showing electron penetration depth of 1 MeV electrons. The four separate figures show the four different sample types as noted in the headings. The dash line represents the sample (to the left of the dashed line) and cold-head (to the right) interface. ....	62
27. Results of CASINO <sup>®</sup> simulation showing electron penetration depth of 0.5 MeV electrons. The four separate figures show the four different sample types as noted in the headings. The dash line represents the MWCNT (to the left of the dashed line) and SiO <sub>2</sub> (to the right) interface. ....	63
28. Results of CASINO <sup>®</sup> simulation showing electron penetration depth of 0.1 and 0.2 MeV electrons. The 2 separate figures show the same sample as noted in the headings. The dash line represents the MWCNT (to the left of the dashed line) and SiO <sub>2</sub> (to the right) interface. ....	64
29. Pre-characterization of EMI Shielding Effectiveness. The thick line represents a Savitzky-Golay smoothing filter of the EMI signal.....	67
30. A comparison of changes to the MWCNT composites post vacuum.. ....	70
31. Changes over time to EMI-SE (left) and conductivity (right) of 4CNT/4GL sample after electron irradiation. ....	72
32. Changes over time to EMI-SE (left) and conductivity (right) of 2CNT/4GL/2CNT sample after electron irradiation.....	73
33. Changes over time to EMI-SE (left) and conductivity (right) of CNT/GLx4 sample after electron irradiation. ....	73
34. A comparison of changes to the MWCNT composites post electron irradiation. The four separate figures show the four different sample types as noted in the headings. ....	74

Figure	Page
35. A potential reaction between CNTs and epoxy resin [48].....	76
36. Changes over time to EMI-SE (left) and conductivity (right) of 4CNT/4GL sample after neutron irradiation. ....	79
37. Changes over time to EMI-SE (left) and conductivity (right) of 2CNT/4GL/2CNT sample after neutron irradiation. ....	79
38. Changes over time to EMI-SE (left) and conductivity (right) of CNT/GLx4 sample after neutron irradiation. ....	80
39. Analysis of variance between pre-characterized conductivity of different sample types.....	81
40. Analysis of variance between pre-characterized, post vacuum and post irradiation conductivity of the different sample types. The three separate figures show the three different sample types as noted in the headings. ....	82
41. Analysis of variance of the 4CNT/4GL .....	83

## List of Tables

Table	Page
1. Baseline standards for proton fluxes of LEO satellites and electron fluxes of geosynchronous satellites listed in [4] .....	6
2. Maximum Energy Transferred.....	24
3. Resistivity of the three copper samples .....	46
4. The effects of skin depths on overall EMI-SE.....	51
5. Electron irradiation operating parameters.....	57
6. OSURR irradiation settings .....	59
7. Conductivity results from vacuum check ( $1 \times 10^{-6}$ Torr) .....	65
8. Effects of Skin Depths on EMI-SE of MWCNT .....	68
9. EMI-SE Vacuum Test.....	69
10. Mean EMI-SE Post Electron Irradiation.....	71
11. Conductivity Post Electron Irradiation ( $1 \times 10^{16}$ electrons/cm <sup>2</sup> @ 500 keV) .....	72
12. Mean EMI-SE Post Neutron Irradiation .....	78
13. Conductivity results Post Neutron Irradiation .....	78

## **List of Symbols and Acronyms**

$\mu\text{m}$	Micrometer [10 <sup>-6</sup> meter]
A	Ampere measure of current
Å	Angstrom [10 <sup>-10</sup> meters]
AFIT	Air Force Institute of Technology
ASTM	American Society for Testing and Materials
CASINO®	Monte Carlo Simulation of Electron Trajectories in Solids
cm	Centimeter [.01 meters]
CNF	Carbon Nano Fiber
CNT	Carbon Nano Tube
CPT	Captain, US Army
EMI	Electromagnetic Interference
ESD	Electrostatic Discharge
ESR	Electron Spin Resonance
eV	Electron Volt
GEO	Geosynchronous Earth Orbit
gsm	Grams per square meter [references nanofiller content]
HDPE	High Density Polyethylene
I	Current [A]
IV	Current verses Voltage
keV	Kilo Electron Volt [10 <sup>3</sup> eV]
kV	Kilo Volt [10 <sup>3</sup> V]
LEO	Low Earth Orbit

mA	Milliamp [ $10^{-3}$ A]
MAJ	Major, U.S. Army
MeV	Mega Electron Volt [ $10^6$ eV]
MIL-STD	Military Standard
MWCNT	Multi Walled Carbon NanoTube
m $\Omega$	Milliohm [ $10^{-3}$ Ohm]
nA	Nanoamp [ $10^{-9}$ A]
NASA	National Aeronautics and Space Administration
NIST	National Institute of Standards and Technology
OSURR	The Ohio State University Research Reactor
rad	Radiation Absorbed Dose
RT	Room Temperature
sec	Second
SWCNT	Single Walled Carbon NanoTube
torr	Measure of Pressure (vacuum) torr = 133.3 Pa
$\rho$	Resistivity [ $\Omega$ -cm]
$\sigma$	Conductivity
$\Omega$	Resistance [ $\Omega$ ]

# DURABILITY OF MWCNT COMPOSITES UNDER ELECTRON AND NEUTRON IRRADIATION

## **I. Introduction**

There is considerable interest in the development of conductive composite materials for application where metals traditionally have been used. The focus of this research is the development of materials intend for use in satellite structural components. Composite materials containing no metallic fillers are electrically resistive and subject to electrostatic discharge (ESD) in the space environment. In order to increase conductivity, fillers such as multi-walled carbon nanotubes (MWCNTs) are added to the composite material. The addition of MWCNTs decreases resistivity in the composite while maintaining its relatively high strength-to-weight ratio

The potential for space use of the MWCNT composites necessitates rigorous radiation effects testing. In addition to radiation from cosmic rays and solar flares, satellites in low earth orbits (LEOs) and geosynchronous orbit are exposed to charged particles trapped in the radiation belts. The charged particles contribute to both spacecraft charging and radiation damage. A detailed understanding of the radiation effects on the electrical properties of the composite is required. The effect of radiation on the composite's conductivity and electromagnetic interference shielding effectiveness (EMI- SE) is the focus of this research. It is also necessary to understand how a material

conducts charge, thus reducing ESD effects, and how well a material can maintain its desirable electrical properties with the effects of permanent radiation damage.

Several studies of MWCNT composites were conducted previously at the Air Force Institute of Technology [1][2]. Changes to the electrical properties of a single layer of MWCNT composite reinforced with a single layer of s-glass were investigated by [1]. The MWCNT composites were irradiated to fluence levels of  $1 \times 10^{16}$  electrons/cm<sup>2</sup> and  $1.11 \times 10^{14}$  neutrons/cm<sup>2</sup>. Reference [1] measured a 3.7 % increase in resistivity post neutron irradiation at fluence of  $1.11 \times 10^{14}$  neutrons/cm<sup>2</sup> and 25.5% increase in resistivity following electron irradiation. Reference [1] concluded that the MWCNT composites were a suitable replacement for aluminum and current composite materials for satellite buses.

Changes to EMI-SE of MWCNT composites after experiencing monotonic tension load, thermal cycling, and a combination of thermal cycling followed by monotonic tension load was investigated by [2]. The materials investigated by [2] are similar to those investigated by [1]. However, [2]'s material consisted of four layers of MWCNT composites and four layers of SiO<sub>2</sub> glass in different configurations. A more detailed description of the material is given in Chapter III. Reference [2] reported that the failure mechanisms were consistent for each MWCNT composite and were not constrained by layered configuration. All three designs containing MWCNT plies did not demonstrate a catastrophic reduction in EMI-SE performance post-fracture. The EMI-SE remained intact after fracture and was able to provide continuing protection against EMI.



## 1.1 Objective of Research

The objective of this work is to investigate the effects of ionizing and non-ionizing radiation on the conductivity and EMI-SE of MWCNT composites. The primary purpose is to determine the effects of a simulated space environment on the composite. Furthermore, since previously reported changes to conductivity following irradiation of single layer CNT composites have been inconsistent, this thesis will also focus on improving the experimental procedures to obtain more dependable results. The primary objectives of this work are as follows:

1. Establish EMI-SE and conductivity test capabilities in accordance with IEEE, Military Standard (MIL-STD), and American Society for Testing Materials (ASTM).
2. Experimentally measure the effect of irradiation on the electrical properties of MWCNT composite materials.
3. Compare the experimental results to the output of a physics-based model of the devices.
4. Attribute results to the interaction of radiation with MWCNTs.

A secondary objective of this work is to determine the radiation effects on MWCNT composites in different layered configuration. The primary object is to measure the changes to the electrical properties of MWCNT composites post electron and neutron irradiation. The purpose of the second objective is to find an optimal stacking sequence for the different composite configurations.

Changes to the electrical properties of nanocomposites after irradiation can be linked to radiation-induced defects in its constituent materials. Reference [1] suggested that the reduction in the conductivity following irradiation is greater due to radiation induced atomic displacements in the CNT. Reference [3], however, suggested that

increase in resistivity in the composite materials was due to changes in the epoxy resin. This research will show that changes to the electrical properties of MWCNT composites under irradiation are due to the following competing processes:

1. Gas absorption and desorption;
2. Radiation induced displacement damage in the MWCNTs; and
3. Radiation induced displacement damage in the epoxy resin.

## **1.2 Paper Organization**

This thesis addresses theory, experimental design, results and analysis, and provides conclusion and recommendations for future work.

Chapter 2 characterizes the problem with space-bound vehicles. It first describes the space radiation environment and defines performance requirements for current spacecraft according to the current MIL-STD.

Chapter 3 discusses the composite material in detail. The first section describes the structure of the carbon nanotubes (CNT) and its' unique properties. The second section describes how MWCNTs conduct electrical currents. In addition, how MWCNT can be infused in epoxy resin to create a conductive composite is also discussed. The third section of the chapter discusses how the conductivity of the composite can change depending on the percent weight of MWCNTs and while under a vacuum environment.

Chapter 4 describes the radiation effects used in this research. The interaction of energetic particles with the MWCNTs is also described. The results of previous studies and how they relate to this research are explained. Understanding the causes and effects of the defects is essential to the development of the radiation effects model.

Chapter 5 describes the experimental techniques used in each of the irradiations and measurements. The first section briefly discusses the tested material and how it was prepared for the experiment. The next several sections discuss resistivity theory, measurement techniques, and experimental set-up. The final few sections discuss EMI-SE theory, measurement techniques and experimental set-up.

Chapter 6 discusses the irradiation of the MWCNT composites. The first section discusses the purpose of a vacuum check and how it was conducted. The second section discusses irradiation of the MWCNT composites with the Dynamitron. The final section describes how irradiation of the composite was done at the Ohio State University Research Reactor (OSURR).

Chapter 7 contains the result and analysis. The first section discusses the initial characterization results and analysis of the EMI-SE and conductivity results. The next section follows the same outline to discuss the results from electron irradiation. Finally, an analysis of neutron irradiation is presented. The first section presents an error analysis of the experimental results.

Chapter 8 offers the conclusion and recommendations for future work.

## II. Characterizing the Problem

### 2.1 The Space Environment

Space applications are of primary interest for the MWCNT composites under investigation. Satellites in geosynchronous orbit circle the earth approximately 35,000 kilometers above the equator in the outer Van Allen radiation belt. Low Earth Orbit (LEO) satellites, on the other hand, circle the earth approximately 2000 kilometers above the earth's equator in the inner Van Allen radiation belt. The radiation belts are composed of a high energy proton belt and two electron belts. The inner belt, located 500 - 13,000 (km) above the earth's surface, contains mostly protons with energy greater than 10 MeV. The low-energy electron belt overlaps the inner belt and contains electrons carrying energies between 10 and 50 MeV. The outer belt, located 13,000 - 35,000 (km), contains high energy electron of energies from 10 to 100 MeV [4]. An illustration of the Van Allen belts is provided in [5].

The baseline proton fluxes for LEO orbits and electron fluxes for geosynchronous

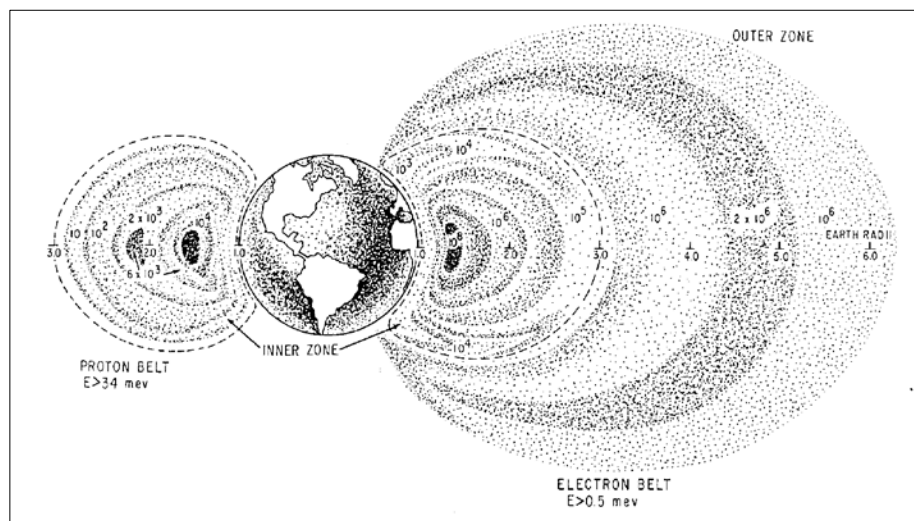


**Figure 1. Van Allen Inner and Outer Belt [5].**

orbits are listed in

Table 1 and were taken from MIL-STD 1809. The document established a standard within which a space vehicle must be capable of operating. The greatest threat facing a space vehicle is protons in the inner belt. Electrons in the outer belt also pose a significant risk. The definition provides an appropriate starting point for radiation fluences used to investigate radiation effects on the electrical properties of carbon nanotube composites. Any material considered for use as structural components on LEO and geosynchronous satellites should meet the criteria outlined in the standard.

**Table 1. Baseline standards for proton fluxes of LEO satellites and electron fluxes of geosynchronous satellites listed in [4].**

<b>Proton Energy [MeV]</b>	<b>Flux [protons cm<sup>-2</sup> sec<sup>-1</sup>]</b>
> 0.1	4x10 <sup>7</sup>
> 1	1x10 <sup>7</sup>
>10	5x10 <sup>5</sup>
>100	2x10 <sup>4</sup>
>400 MeV	8x10 <sup>2</sup>
<b>Electron Energy [MeV]</b>	<b>Flux [electrons cm<sup>-2</sup> sec<sup>-1</sup>]</b>
> 0.1	2x10 <sup>7</sup>
> 0.5	8x10 <sup>6</sup>
> 1	2x10 <sup>6</sup>
> 2	2x10 <sup>4</sup>

Space vehicles in LEO and geosynchronous orbit experience a multitude of high energy particles as detailed above. This investigation will examine both the spacecraft charging and radiation effects on the electrical properties of the satellite buses. Space vehicle charging will be discussed presently, while the discussion of radiation effects on electrical properties will be deferred until a complete description of the composite materials has been presented.

## 2.2 Space Vehicle Charging

One of the hazards caused by radiation is spacecraft or satellite electrical charging. There are three ways that charging can be produced:

1. By space vehicle motion through a medium containing charged particles (“wake charging”). Wake charging is a significant problem for large objects such as the Space Shuttle or International Space Station.
2. Directed particle bombardment from geomagnetic storms and proton events.
3. Solar radiation, which causes time dependent ionization

The material used, and the shape of the space vehicle’s construction can influence the impact of the vehicle charging [6]. Unbalanced electrical potential between the separate surface components of the vehicle or between vehicle and surrounding plasma are created from a buildup of charge density. The buildup of large static charge eventually leads to an ESD. There are two types of charging:

1. Surface charging occurs when low energy electrons attach to the spacecraft causing different charges on parts of the spacecraft leading to an electrical arc discharge on the surface. Photoelectric effects from solar photons and wake charging are surface charging phenomena.
2. Deep dielectric charging occurs when high energy electrons penetrate through the shielding of the spacecraft and build up in dielectric insulators and conductors such as coaxial cable.

Surface ESD can produce spurious circuit switching, degradation or failure of internal electronic components, thermal coatings, and solar cells, or false sensor readings [6]. The primary concern with using composite material is their low conductivity. Conductive structural materials reduce the uneven charge buildup across the satellite surface and reduce the possibility of ESD. Infusing epoxy with MWCNT can

significantly increase the conductivity of the material and thus reduce the likelihood of an uneven charge buildup.

### III. The Material

Since the discovery of carbon nanotubes in 1991 by [7], researchers in various fields such as physics and material science have looked extensively for potential applications. Applications such as electrostatically dissipative materials and satellite structural materials are one such area of interest. CNTs' remarkable electrical and mechanical properties have inspired interest in using CNTs as fillers in polymer composite systems to obtain ultra-light structural materials with enhanced electrical, thermal and optical characteristics. The prospect of obtaining advanced CNTs with multifunctional features has attracted the efforts of researchers in both academia and industry.

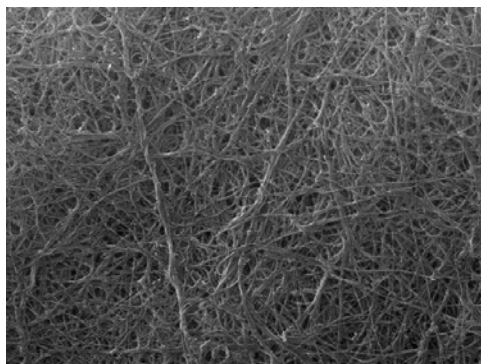


**Figure 2. 90 wt% Multi-walled Carbon Nanotube Bucky Paper [8].**

Nanocomp Technologies, Inc. (NCTI) based in Concord, New Hampshire fabricated the MWCNT bucky paper used in this research via Chemical Vapor Deposition (CVD). The bucky paper or sheets of MWCNT were then infused with epoxy resin. Finally, the MWCNT and epoxy resin layers were then compressed onto layers of SiO<sub>2</sub> glass to form different configurations. An image of the MWCNT produced by NCTI is shown in Figure 2.



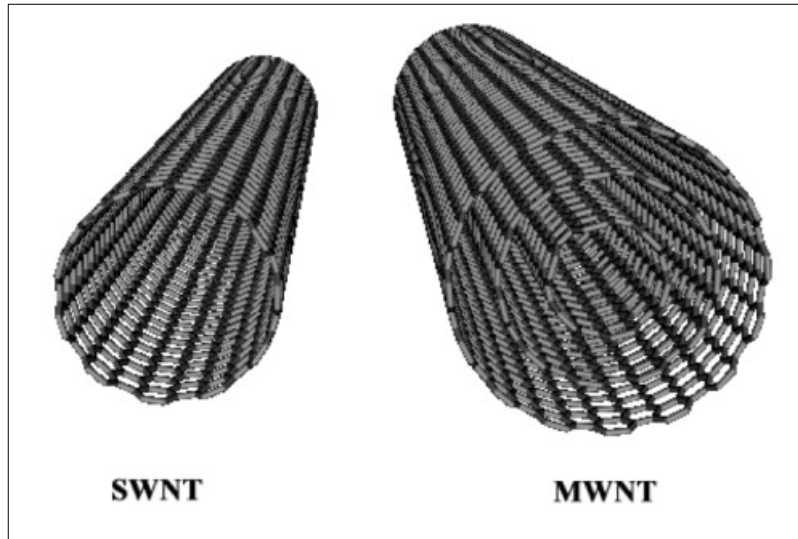


**Figure 3. SWCNT and MWCNT [9].**

### 3.1 Carbon Nanotubes

Carbon nanotubes consist of a hexagonal network of carbon atoms rolled up into a continuous hollow cylinder. Each end can be either open or capped with half of a fullerene molecule. Carbon nanotubes can be single-walled, double-walled or multi-walled. MWCNT and DWCNT are essentially nested SWCNT. Each configuration has its own unique electrical and mechanical properties. Figure 3 depicts a SWCNT and a nested CNT.

Each carbon atom in the CNT is bonded to three neighboring carbon atoms. The structure is due to the process of  $sp^2$  hybridization during which one s-orbital and two p-orbitals combine to form three hybrid  $sp^2$ -orbitals. Figure 4 depicts how the  $sp^2$ -orbitals of the carbon atom connect to  $sp^2$ -orbitals of neighboring atoms to form a hexagonal network. The covalent bond or  $\sigma$ -bond is a strong chemical bond and plays a vital role in the mechanical properties of the CNTs. In addition, the out-of plane bond or  $\pi$ -bond is

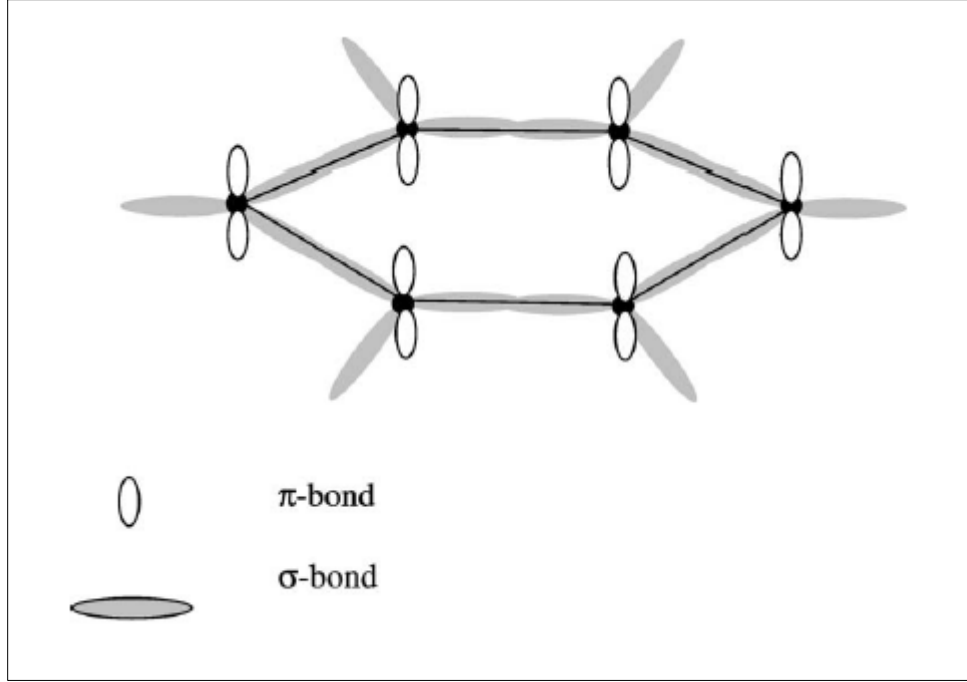


**Figure 4. Hybrid  $sp^2$ -orbitals of carbon atoms forming a hexagonal network. The carbon  $\pi$ -bonds contribute to the interaction between layers of MWCNT and bundle of CNTs [11] .**

relatively weak and contributes to the interaction between the layers in MWCNTs or between bundles of CNT's [10].

The bonds of CNTs are similar to those in graphene sheets; however, rolling up a sheet of graphene into CNTs re-hybridizes the  $\sigma$  and  $\pi$  orbitals [10]. CNTs can also be identified by how the graphene sheets are rolled as shown in Figure 5. The identification is based on the vector  $\mathbf{r}$  which can be expressed as the linear combination of the lattice basis ( $\mathbf{a}$  and  $\mathbf{b}$ ). As shown in Figure 5,

$$\mathbf{r} = N\mathbf{a} + M\mathbf{b} \quad (\text{III.1})$$

The relation between N and M defines the three categories of CNTs:

- $M = 0$ : *Zigzag*

- $M = N$ : *Armchair*
- $M \neq N$ : *Chiral*

The armchair structure has metallic characteristics while both zigzag and chiral structures result in band gaps, making them semiconductors. The nanotube's chirality and its diameter determine its unique electrical properties [11].

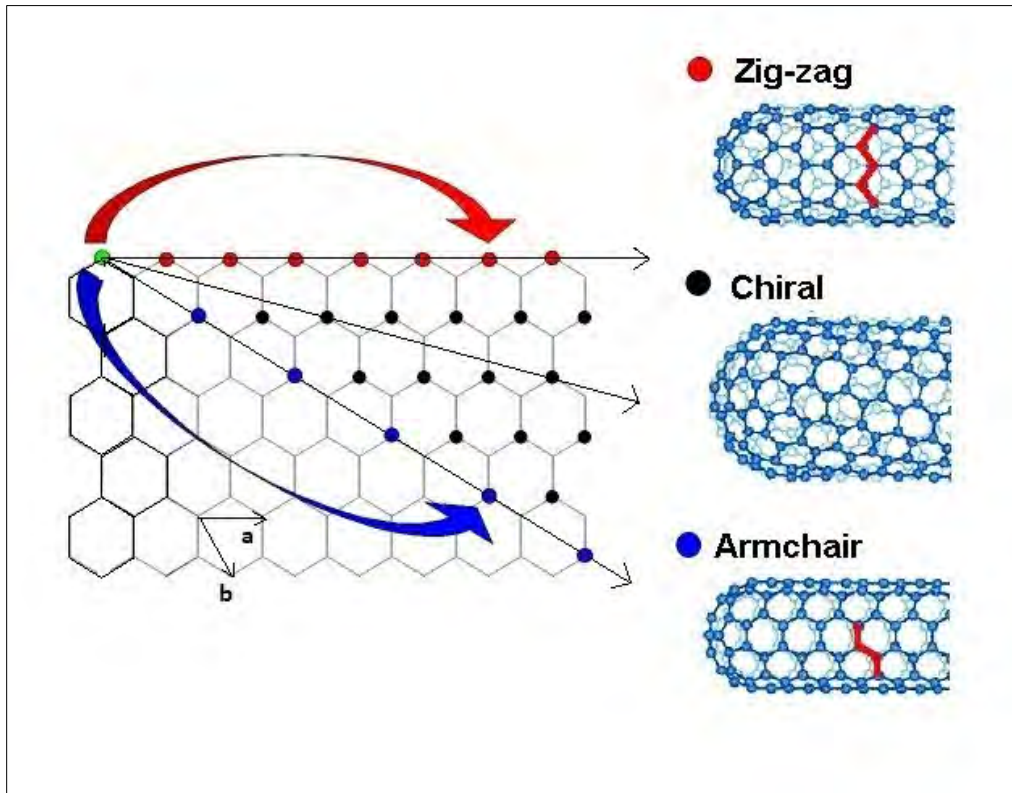


**Figure 5. The rolling of a graphene sheet determines the three types of CNT [32].**

### 3.2 Epoxy Resin Polymer

Epoxyes are used primarily for fabricating high performance composites with superior mechanical properties, resistance to corrosive liquids and environments, superior electrical properties, good performance at elevated temperatures, good adhesion to a

substrate, or a combination of these benefits. Epoxy resins can be used with a number of fibrous reinforcing materials including glass, carbon and aramid fibers.

Epoxy resin polymer is formed from the reaction of an epoxy and amine molecule. The “resin” or “compound” consist of monomers or short chain polymers with an epoxy group at either end. The “hardener or “activator” consists of polyamine monomers. When these two compounds are mixed together, the amine groups react with an epoxy group. The resulting polymer is heavily cross-linked which makes it strong and rigid.

### **3.3 Composite Material**

Composite materials are made of more than one component. A common composite is concrete which is made of cement, gravel and sand. The concrete is often reinforced with interconnecting steel rods. Modern composites are usually made of two components, a fiber and matrix. The fiber can be glass, Kevlar, carbon fiber, or polyethylene. The matrix is usually an epoxy resin or polyimide. The fiber is embedded in the matrix in order to make the matrix stronger. Fiber-reinforced composites can be stronger than steel and much lighter. Similarly, the CNT composite consists of an epoxy resin matrix reinforced with interconnecting CNT filler. The CNT provides the composite increased structural strength and conductivity. The increased structural strength and electrical conductivity of the MWCNT composites make it an ideal replacement for aluminum and other heavier alloys in satellite buses.

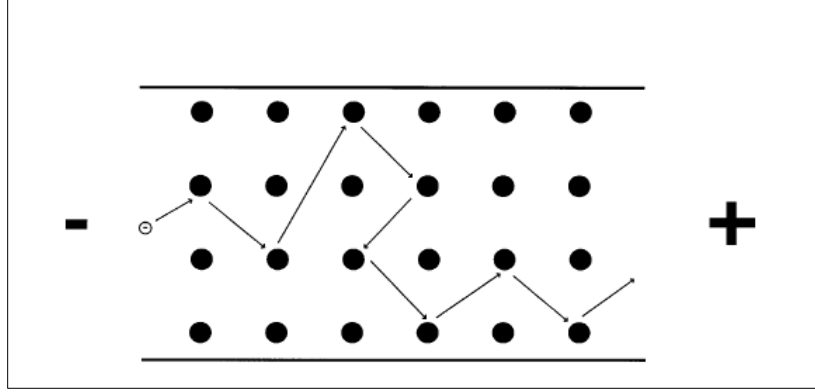


**Figure 6. Simple model of electron flow in material. The white circle represents an electron moving from the left to the right through the atoms of the material [12].**

### 3.4 Electrical Conductivity of MWCNT

**Electrical conductivity is a key physical property of all materials. The electrical conductivity describes the flow of electricity in material when under an applied voltage. If electricity can flow easily through a material, that material has high conductivity and vice versa. Electric current flow is often viewed as an electron response to an applied electric field.**

Figure 6 is a basic model of how electricity flows through a material under an applied voltage.

For CNTs, electron transport is often considered as a scattering problem. In this approach, the current through a conductor is related to the probability that an electron can be transmitted through it. Landauer formula relates the conductance  $G$  over a sample of length  $L$  as

$$G = \frac{\sigma}{L} = \frac{2e^2}{h} T \quad (\text{III.2})$$

where  $h$  = plank's constant

$e$  = the electric charge on an electron

$T$  = the transmission coefficient

The transmission coefficient  $T$  is proportional to the ratio of the overall scattering length and the length of the system,  $v_F\tau_m/L$ . The scattering length,  $v_F\tau_m$ , consists of the Fermi velocity,  $v_F$ , and the  $\tau_m$ , which takes into account many body collisions that redistribute the carriers' energy gain and cause dissipation. A change in the transmission coefficient changes the conductance of the material [12].

### 3.5 Conductivity of MWCNT composites

The electrons in the  $\pi$  orbital of the CNT play a significant role in the conductivity of MWCNT composites. The loosely bound  $\pi$  electrons in MWCNT provide the current carrying electrons in the composites. The MWCNT composites' high conductivity makes them ideal fillers for creating conductive composites. Infusing the MWCNTs with epoxy resin turns a normally resistive material into a highly conducting composite. There are several ways to influence the flow of electricity through MWCNT composites. One way to increase the conductivity of the material is to create additional charge carrier transport pathways. This can be done by adding more MWCNTs to the matrix material.

When electrically conducting particles are randomly distributed within an insulating matrix, the sample is non-conducting until the volume fraction of the conducting phase reaches the so-called percolation threshold [14]. Figure 7 shows the percolation thresholds of MWCNT/epoxy nanocomposites which can vary from 0.06 % to above 0.64% depending on dispersion and aspect ratio (length to diameter) of MWCNTs and how it is produced [14].

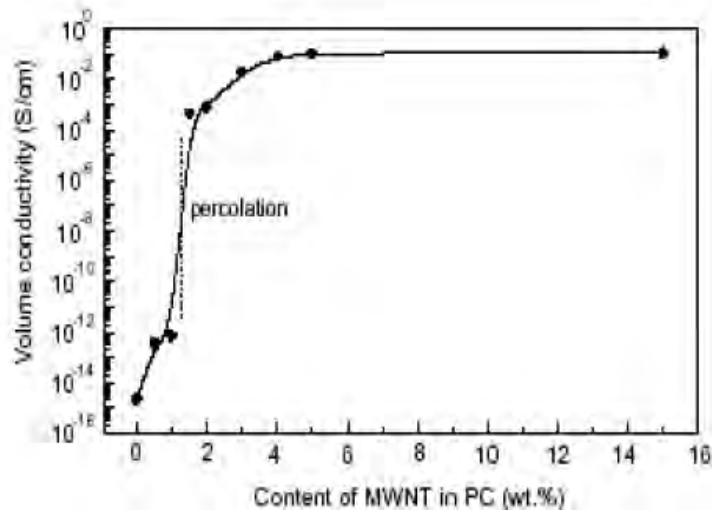


**Figure 7. Percolation level of MWCNT composites [14].**

In classical percolation theory, the dependence of the DC conductivity ( $\sigma$ ) values of the composites on the conductive filler concentration ( $p$ ) above the percolation concentration ( $p_c$ ) can be describe by a scaling law of the form

$$\sigma \propto (p - p_c)^t \quad (\text{III.3})$$

where  $t$  the critical exponent. The theoretical predictions of  $t$  have been reported ranging from 1.6 to 2.0 [14] [15].

When  $p \gg p_c$ , small changes in  $p$  have little changes in the overall conductivity of the composite. Figure 8 shows a comparison of the DC conductivity for two samples of MWCNT composites. Reference [16] reported that the percolation threshold of each composite can occur at different MWCNT content depending on the oxidation condition and solution [16]. The composites showed different conductivities even at the same MWCNT content. An abrupt increment in conductivity was observed at low MWCNT content in both cases, at which point the conductivity changed from the order of  $10^{-15}$  to  $10^{-6}$  S/cm. At loading levels of more than the critical volume, the

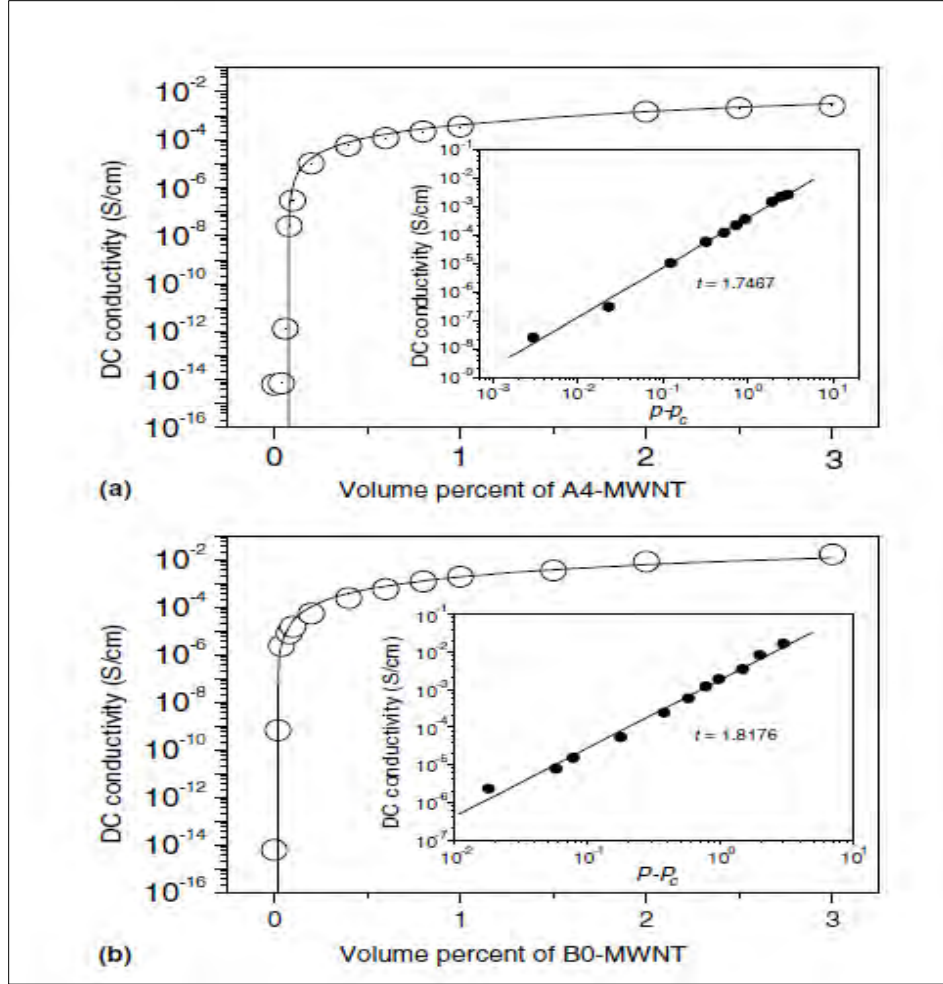


**Figure 8. Plot of DC conductivity of two types of MWCNT composite as a function of MWCNT content. Each inset shows the log-log plot of DC conductivity with  $p-p_c$ .**

conductivity of the epoxy composites was moderately increased and saturated to a value of less than 0.01 S/cm [14].

### 3.6 Gas Absorption/Desorption Model of MWCNT Composites

Figure 9 depicts a model that describes the adsorption/desorption of a Carbon Nano Fiber (CNF) and the associated carrier trapping/detrapping under ambient and vacuum conditions. The model assumes the adsorption of one or more gaseous species in



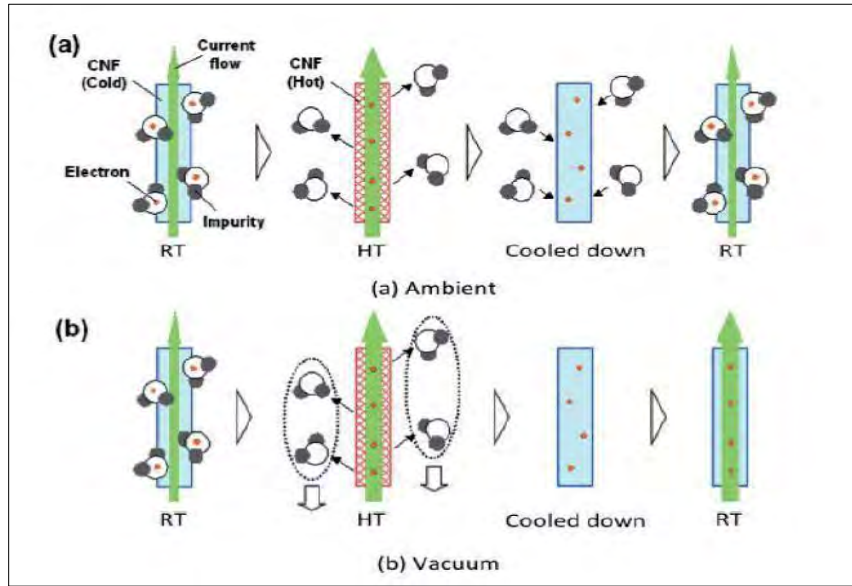


**Figure 9. Gas Absorption/Desorption Model [17].**

the atmosphere at room temperature, which desorbed via Joule heating of the CNF device under ambient conditions, accompanied by release of carriers into the CNF. Once the CNF is cooled to room temperature, the molecules are re-adsorbed and the resistance returned to its preheated value. If the heating occurs in vacuum, the desorbed molecules are evacuated and the resistance after cooling down remains at the lower value. The model proposed is consistent with reports on effects of adsorbed molecular species such as  $O_2$ ,  $H_2O$ ,  $NH_3$ ,  $CO_2$ , and  $NO_2$  on electrical transport in CNTs. The general trend reported was increased CNT resistance as a result of exposure to reducing species ( $NH_3$ ,  $CO_2$ ), while a decrease was observed for oxidizers ( $O_2$ ,  $NO_2$ ) [17].

Changes to the electrical properties of MWCNT composites can be attributed to the adsorption and desorption of gas molecules in the atmosphere. Theoretical work has shown that electronic properties of CNTs change in the presence of absorbed reducing and oxidizing gases [18]. Reference [17] reported that absorbed molecules can be

desorbed through heating, resulting in a decreased resistance. The resistance returns to its original value due to re-adsorption of these molecules. The exposure to O<sub>2</sub> (electron acceptors) was reported to result in decreased resistance. Water vapor has been reported to increase resistance in small concentrations for single-walled CNT mats. The same authors also found that degassing while heating CNT mats resulted in reduced resistance [19]. CO<sub>2</sub> gas present in the atmosphere and exposure to it were reported to increase the multi-walled CNT resistance [20]. These results were typically explained based on the assumption that absorbed gas molecule act as electron (or hole) donors or acceptors.

#### **IV. Model for Radiation Effects**

A full understanding of irradiation effects in MWCNT composite is not possible without a proper description of the target atom and its interaction with an energetic ion or electron. The purpose of this section is to examine the fundamentals of the interactions between the target atoms and energetic particles that modify the properties of the MWCNT composite.

Radiation effects on MWCNTs and CNTs in general are significantly different from bulk carbon systems (graphite and diamond). Unlike bulk systems, the radiation can have both a destructive and beneficial effect on the target's properties. Initial effects of radiation on MWCNT composite material can be generalized into two categories, ionizing and non-ionizing effects. When electrons or neutrons enter MWCNT composite material, there are three possible outcomes. The first possible outcome is that the energetic particles pass through the material with no energy loss. The second possible outcome is that the particles (if charged) lose their energy through ionization. The ionization energy loss is transitory and rate dependent. The third possible outcome is that the particles lose their energy through non-ionizing energy loss (NIEL). NIEL is typically manifested as the displacement of constituent atoms leading to vacancies, interstitials and the creation of defect complexes. The NIEL effect is potentially permanent and generally dependent upon total dose rather than dose rate [21] .

The electronic structure of the MWCNT strongly affects the outcome of the radiation interaction. In metallic materials, the electronic excitations are delocalized due to the presence of conduction electrons [29] . When electrons in MWCNT are excited, the energy of the electron is quickly transferred to other electrons before it creates any

permanent damage. Hence ionizing effects on MWCNT are transient. Any permanent damage can be attributed to the radiation induced changes in carbon nanotubes by NIEL. NIEL is a measure of the energy transferred to the atoms of the lattice during irradiation [23]. The effect of the energetic particles on the constituent atoms of the material differs depending on the atomic species, binding energy, and energy of the particles [21]. The potential effects of the type and energy of the incident radiation can be determined by analyzing the potential energy transfer to the lattice atoms. Additionally, in order to determine the NIEL in a material, a calculation of the radiation dose for the energy level of the radiating particles is required.

#### **4.1 Neutron Non-Ionizing Energy Loss**

When an energetic neutron penetrates a solid, it interacts with the nuclei and the electrons of the material. The neutron is difficult to stop and has a high penetrating power because it has no charge. Interactions of neutrons with the target atom nuclei fall into two broad classes, scattering and absorption. In scattering reactions, the neutron remains free at a reduced energy and some of its kinetic energy is transferred to the nuclei. The neutron transfers its energy in two different processes: ionizing and nonionizing. The ionizing effect is governed by inelastic collisions between the neutron and the bound or free electrons in the target [23]. The nonionizing effect originates from elastic collisions between the neutron and the nuclei of atom in the target atom. If the neutron is absorbed, a new isotope is formed [21].

The 1 MeV equivalent neutron fluence for a material or 1 MeV (eq) is reported for the purpose of radiation testing. The 1 MeV (eq) is the fluence required for 1 MeV

mono-energetic neutrons to create the same amount of damage as the entire neutron spectrum. MIL-STD-75D METHOD 1017.1 is used to determine the 1 MeV (eq) while the ASTM E722 (1994) standard outlines the approved method. The damage effectiveness equivalence of the entire neutron source spectrum is reduced to a monoenergetic source in order to determine the displacement damage effectiveness of the entire neutron energy spectrum.

In order to limit the damage to only fast neutrons, all samples were enclosed in a cadmium case before exposure to the reactor neutrons. Neutron energies below 0.45 eV were assumed to be absorbed by the cadmium and not included in the neutron fluence. The 1 MeV equivalent mono-energetic neutron fluence,  $\Phi_{eq,1MeV,Mat}$  is found using Equation IV.1.

$$\Phi_{eq,1MeV,Mat} = \frac{\int_0^{\infty} \Phi(E) F_{D,Mat}(E) dE}{F_{D,1MeV,Mat}} \quad (IV.1)$$

where  $\Phi(E)$  is the incident neutron energy-fluence spectral distribution,  $F_{D,Mat}$  is the neutron displacement damage function for the irradiated material as a function of energy, and  $F_{D,1MeV,Mat}$  is the displacement damage reference value designated for the material for 1 MeV.

## 4.2 Electron Irradiation

Coulomb scattering is the primary interaction between an electron and a target atom. The interaction can lead to both excitation and liberation of atomic electrons. In addition, sufficient energy can be transferred to displace the target atom from its normal

lattice positions [21]. The rate of displacement damage formation on MWCNT composites lattice structure depends on both the displacement energy and the maximum transferable energy during collisions [23]. The displacement energy depends on both the energy binding the atom to the lattice and the angle of the interaction. The fraction of energy transferred depends on the mass of the nucleus. The transfer energy  $E^{tran}$  can be expressed as

$$E^{tran} = E_{tran}^{max} \cos^2 \theta \quad (IV.2)$$

where  $\theta$  is the angle between the initial direction of the electron motion and the direction of the scattered atom motion. The maximum energy is transferred in a head-on collision ( $\theta = 0$ ). The recoil atom can acquire the maximum energy given by

$$E_{tran}^{max} = 2 \frac{(E_e + 2m_e c^2)}{m_{atom} c^2} E_e \quad (IV.3)$$

where the  $E_{tran}^{max}$  value for each of the component of the MWCNT composite is shown in Table 2. For low electron energies, or when  $\theta$  is large, the initial kinetic energy of the recoil atom is too small to overcome the lattice binding energy, so the electron impact causes atomic vibration. If the electron imparts enough energy to the recoil carbon atom to overcome the lattice binding energy, the atom can be dislodged from its position in the lattice. The probability that a carbon atom will recoil with enough energy to become dislocated is determined by the displacement cross section. The displacement cross section  $\sigma$  is a function of energy and particle type. An electron of energy  $E$  traveling a distance  $dx$  in a material with  $N$  atoms per unit volume will have a probability  $P$  of

collision with a host atom proportional to  $\sigma$ ,  $dx$  and  $N$ . The displacement cross section can then be used to estimate the number of defects produced in an irradiating flux of electrons [23].

The displacement energies of the constituents of MWCNT composites are also listed in Table 2. The displacement energy of MWCNT calculated by [24] was between 15 to 20 eV. The displacement energy is dependent on the diameter and chirality of the nanotube. The displacement energies for oxygen, nitrogen and carbon in the epoxy were taken from the Stopping and Range of Ions in Matter (SRIM) software. For the purpose of comparison and to evaluate how the SiO<sub>2</sub> glass is affected by the electron irradiation, the maximum energy transferred to silicon was also calculated.

**Table 2. Maximum Energy Transferred**

Incident Energy (MeV)	Max Energy Transferred to Carbon Atom (eV)	Max Energy Transferred to Hydrogen Atom (eV)	Max Energy Transferred to Oxygen Atom (eV)	Max Energy Transferred to Nitrogen Atom (eV)	Max Energy Transferred to Silicon Atom (eV)
0.1	20	241	15	17	9
0.2	44	525	33	37	19
0.5	136	1634	102	117	58.3
Displacement Energy (eV)	15-20	3	21	20	25

### 4.3 Radiation Effects on MWCNT Composites

During the course of this research, the MWCNT composite was exposed to electron and neutron irradiation. Associated with these radiation sources are also x-ray and gamma radiation. In order to determine the effects of radiation on the properties of MWCNT composites, we need an understanding of the current state of knowledge

regarding the defects caused by radiation on the constituent materials. The purpose of this section is to discuss the effects of radiation induced defects on epoxy resin and carbon nanotubes.

#### **4.4 Radiation Effects on Epoxy Resin**

Generally, equivalent dose gives equal damage regardless of the radiation type in the epoxy resin. Charged particles with energy above the electron binding energy eject an electron from the atom, resulting in ionization. Particles with energies below the binding energy may form excited states that generate free radicals or other chemical species. Gamma rays produce electrons by Compton scattering while neutrons may contribute to ionization from recoil ions. Regardless of the type of radiation, when the incident particle or photon interacts with the epoxy resin, it generates reactive, transient intermediate free radicals. Radiolytic hydrogen gas from ruptured C-H bonds is formed in the epoxy resin. The reactive radicals formed will interact with one another. If there are fillers in the media, such as carbon nanotubes, the fillers will also react with those agents [27].

Materials exposed in a reactor are subjected to both neutrons and gamma rays. Irradiation can permanently alter the electrical properties of epoxy resin systems due either to chain scission or to cross-linking. Cross-links result in decreased elongation, increased tensile strength, and increased modulus. Chain scissions result in brittleness, fracturing, gas generation and de-polymerization. An increased in conductivity of the epoxy resin indicating the production of ions or changes in the structure after irradiation was reported by [28]. A decreased DC conductivity measurement after annealing also provides evidence that structural effects are not the entire explanation for the changes



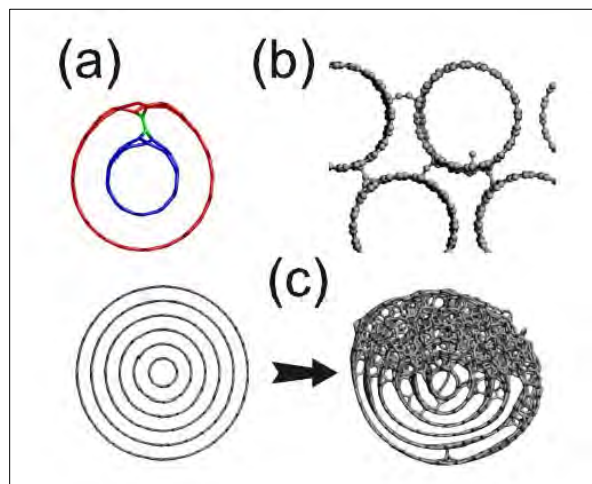


**Figure 10. Radiation induced damage in MWCNT and CNT bundles [23].**

from irradiation. Discharging of species during the irradiation is also a factor. A possible degradation mechanism is the occurrence of dimensional changes of the resin which could accompany cross-link, scission and/or evolution of gaseous radiolysis products. The breakdown of composite properties may involve destruction of the bulk resin matrix.

#### **4.5 Radiation Effects on Carbon Nanotube**

Radiation effects on carbon nanotubes can be classified into two categories: effects caused by ion irradiation and those caused by electron irradiation [25]. Effects of electron irradiation on carbon nanotubes using Transmission Electron Microscope (TEM) have been studied extensively [23] [24] [25] [26]. A TEM can be used to create damage in the nanotubes in a controllable manner and monitor the irradiation effects. Effects of ion irradiation on CNTs have also been studied extensively [29] [30]. Ion irradiation of CNT is also classified into two categories. The two categories are split between light and heavy ions. Neutron, protons, helium and lithium ions are referred to as light, while other chemical elements are treated as heavy ions. Both electron and ion irradiation induces

defects on to the CNTs. In addition to the simple point defects, a number of more complex defects can be formed in MWCNTs. Examples of these defects are inter-shell covalent bonds in MWCNTs. Likewise, defect mediated covalent bonds between CNT bundles can also appear. Figure 10 depicts the different types of defects that can appear. The next several sections will examine recent studies conducted on the radiation effects on CNTs.

#### **4.5.1 Experimental Studies (Electrons)**

Early studies have shown that SWNTs exposed to focused electron irradiation were deformed and developed neck-like features due to removal of carbon atoms by knock-on displacements [23]. Experimental studies demonstrated that the electron energy creates defects non-uniformly. When the electron energy is not very high above the displacement energy, carbon atoms are most rapidly knocked off from surfaces lying normal to the beam. For higher energies, large-angle scattering dominates because of a higher cross-section. Figure 10b shows how CNTs in bundles developed cross links between CNTs when irradiated with moderate doses. The result was a one to two order of magnitude increase in the bundle's conductivity [23]. Figure 10a shows the formation of covalent bonds between the tube bundles which can also enhance the inter-tube conductance. Figure 10c shows that at higher doses the crystalline structure of the MWCNT become amorphous, which decreases the conductivity of each tube. Similar to SWCNTs, electron irradiation of MWCNTs resulted in the formation of vacancies on the walls and subsequent destruction upon high-dose irradiation. MWCNTs are more stable under electron irradiation than SWCNTs because atoms sputtered from inner shells

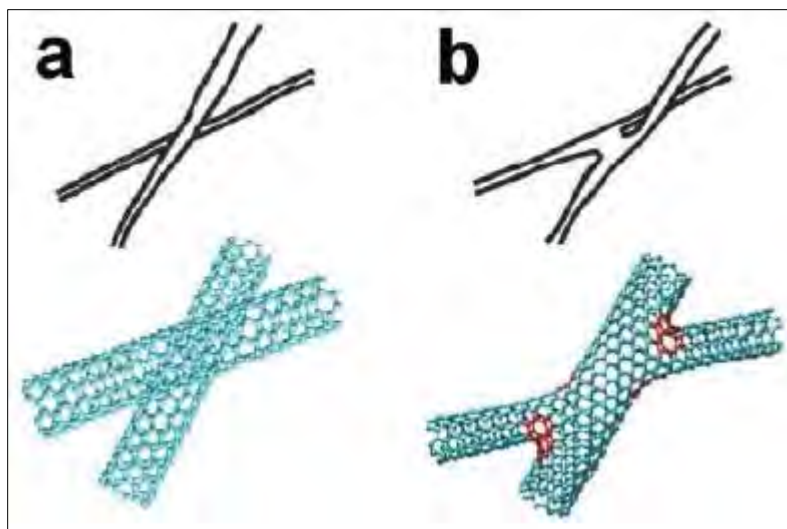


**Figure 11. Irradiation gives rise to current redistribution between the damaged and undamaged tubes [23].**

remain in the MWCNT, and Frenkel pairs created inside the MWNT can easily recombine [23].

#### **4.5.2 Experimental Studies (Ions Irradiation)**

The impact of low-dose ion irradiation on bundles of SWNTs has been experimentally studied [29]. The result suggests that irradiation gives rise to current redistribution between the damaged and undamaged tubes, which can be interpreted as evidence for the formation of irradiation-mediated links between individual MWCNTs in the bundle. Figure 11 is an example of the phenomena. The links appear to be of the same origin as the inter-tube links in electron-irradiated nanotube bundles. The formation of covalent bonds between bundled-up nanotubes under impacts of low energy ions was also reported by [24].

### **4.5.3 Light ions: Proton Irradiation of Carbon Nanotubes**

Experiment with high energy protons have recently been carried out and report by [29]. Bucky paper, which represents a highly interconnected network of SWCNTs, was irradiated with high-energy protons. Effects of the irradiation on the nanotubes embedded into a polymer matrix were studied as well. The interest in the response of nanotubes to proton irradiation was stimulated by the possible use of nanotubes in space applications, in particular as components of solar cells.

The irradiation of MWCNT with 2 MeV protons causing the room temperature resistivity of the carbon nanotube bucky paper samples to increase nearly linearly up to a fluence of  $7 \times 10^{16}$  ions/cm<sup>2</sup> was reported by [32]. Irradiation doses  $\geq 10^{16}$  protons/cm<sup>2</sup> completely destroyed the crystalline structure of the CNT sample. At lower dose, fusing of nanotubes can occur similar to the welding induced by a focused electron beam. Irradiation of overlapping nanotubes resulted in welding of nanotubes. Light ion irradiation of nanotubes on a substrate also resulted in the pinning of the nanotubes to metallic, graphite and silicon substrates. Irradiation-induced defects develop chemical bonds between the nanotube and substrate atoms thus increasing the nanotube-substrate adhesion.

## **4.6 Summary**

The space environment as defined in [4] and [27] in conjunction with the work from [1], [2], and [3] provided a starting point for material preparation, choosing irradiation levels for testing, and deciding on specific measurement techniques to employ

in this investigation. The radiation tolerances that satellite structural materials must meet provided a good starting point for irradiation levels to investigate.

## V. Experimental Procedure

### 5.1 Experiment Overview

This experiment measured radiation effects to the in bulk conductivity and electromagnetic interference shielding effectiveness of four panels; three panels consisting of MWCNT composites and SiO<sub>2</sub> glass in different layered arrangements, and one panel consisting entirely of SiO<sub>2</sub> glass. EMI-SE and bulk resistivity of samples cut from the four panels were measured before and after irradiation with 0.5 MeV electrons. Pre and post EMI-SE and bulk conductivity of a second set of samples were measured after 1.0 MeV Si (eq) neutron irradiation.

### 5.2 Description of the Tested Material

Nanocomp Technologies, Inc. (NCTI) manufactured all four panel used in this research. Each individual nanocomposite panel is described along with the same shorthand used in [2]. Four, 929 cm<sup>2</sup> panels were constructed from Cycom 5575-2 glass with MWCNT layers as illustrated Figure 12. Cycom 5575-2 glass is a space grade glass manufactured from SiO<sub>2</sub>. The first panel was made entirely from layers of SiO<sub>2</sub> glass with no MWCNT and will be referred to as *8G*. The second panel was made with four layers of MWCNT plies and four SiO<sub>2</sub> glass layers and will be referred to as *4G/4CNT*. The third panel was made with two layers of MWCNT composite on the exterior and four layers of glass in the interior. This configuration will be referred to as *2CNT/4G/2CNT*. The fourth configuration had alternating layers of MWCNT composite and glass and will be referred to as *G/CNT×4*.

Glass	Glass	CNT	Glass
Glass	Glass	CNT	CNT
Glass	Glass	Glass	Glass
Glass	Glass	Glass	CNT
Glass	CNT	Glass	Glass
Glass	CNT	Glass	CNT
Glass	CNT	CNT	Glass
Glass	CNT	CNT	CNT

*8G*

*4G/4CNT*

*2CNT/4G/2CNT*

*G/CNT<sub>x4</sub>*

**Figure 12. Stacking Configuration of MWCNT Composites**

All four, 8-ply test panels had a 3-harness satin weave, Astroquartz II (S-glass) fabric made from high purity 99.95% SiO<sub>2</sub> quartz crystals with Cycom 5575-2 cyanate ester prepared resin. The three designs having carbon nanotubes (CNT) utilized multi-walled CNTs (MWCNT) with an estimated length of 700  $\mu\text{m}$ , diameter 8 - 15 nm, 90 wt %, and a concentration of 18.3 grams/m<sup>2</sup> (GSM) of MWCNTs. The MWCNT bucky paper contained no matrix material and was made entirely of MWCNTs. The average MWCNT/epoxy layer thickness was 84.89  $\mu\text{m}$ . The average glass layer thickness was 212.53  $\mu\text{m}$  and the average total thickness was 1.215 mm.

Eight panels of 7.0 cm  $\times$  2.54 cm (3 in  $\times$  1 in) strips were cut with a diamond saw. In addition, 8 sticks of 20 mm  $\times$  2 mm were cut from the 8 panels for 4 probe resistivity measurements. The dimensions and preparation procedures were chosen to follow as closely as possible to those reported in [1] and [3] in order to reduce the likelihood of introducing changes that may affect measurements and to provide for the most accurate comparison to previous results. Conductivity and EMI-SE measurement fixtures restricted the maximum sample sizes that could be measured. Moreover, the beam area for the electron beam from the Dynamitron also limited the maximum useful

sample size to a 2.74 cm diameter. Each 7 cm × 2.54 cm test specimen was cleaned with isopropyl alcohol immediately after machining to eliminate undesirable fragments.

### **5.3 Resistivity Measurements**

#### **5.3.1 Theoretical and Historical Consideration**

The purpose of this section is to provide a historical and theoretical development of resistivity measurements. There has been considerable confusion in both literature and current research on resistivity measurements. The confusion resulted from using the term “ohms per square” or “ohms per cm” to describe the surface resistivity of materials. The ESD Association describes surface resistivity in the following way: “For an electric current flowing across a surface, the ratio of DC voltage drop per unit length to the surface current per width.” Basically, the surface resistivity is the resistance between two opposite sides of a square and is independent of the size of the square or its dimensional units. Thus surface resistivity is expressed in ohms per square. However, when using a concentric ring fixture, surface resistance is given in ohms.

A historical account on the source of this inconsistency was given by [36]. In 1954, [33] wrote about the four-point probe method to make surface resistivity measurement on germanium transistors. Both the work of [33] and [34] assumed a three-dimensional structure with one infinite dimension. The work of [33] and [34] were expanded by Smits in 1958. Reference [35] defined a four-point probe method that has become the semiconductor industry standard of measuring resistivity [36]. In that publication, Smits develop the method of measuring the sheet resistivity of diffuse layers



on various samples. He started with a current source in an infinite sheet which gives rise to the logarithmic potential

$$\varphi - \varphi_0 = -\frac{I\rho_s}{2\pi} \ln r \quad (\text{V.1})$$

where:  $\varphi$  = the potential,

$I$  = current,

$\rho_s$  = sheet resistivity, and

$r$  = the distance from the current source.

A potential for a dipole then becomes

$$\varphi - \varphi_0 = -\frac{I\rho_s}{2\pi} \ln \frac{r_1}{r_2} \quad (\text{V.2})$$

where  $r_1$  and  $r_2$  are the distance from the current source. In the case of the four point probe on an infinite sheet, the two outside points represent a dipole. The potential difference between the two inner points then becomes

$$\Delta\varphi = V = -\frac{I\rho_s}{\pi} \ln 2 \quad (\text{V.3})$$

and can be rewritten as

$$\rho_s = \Delta\varphi = \frac{V}{I} \frac{\pi}{\ln 2}. \quad (\text{V.4})$$

In the case of a finite sheet, the method of images can be applied. Reference [35] made several assumptions in order to apply the method of images. He assumed that only non-conducting boundaries and equal spacing probes are considered. In addition, he assumed that the boundary edges of the diffuse layer must be etched to prevent the back side of the sample from acting as an alternate current path. Figure 13 is a depiction of the four point

The equation gives the potential distribution for an infinites number of current sources, arranged in a line and equally spaced [35] . With this expression, the problem is reduced to a summation of lines of current sources with alternating sign in only one direction. In

the coordinate system, for every line of sources, the points 1 and 2 have the x-coordinate zero. The expression simplifies to

$$\varphi - \varphi_o = -\frac{I\rho_s}{2\pi} \ln\left(e^{\frac{\pi y}{d}} - e^{\frac{-\pi y}{d}}\right). \quad (\text{V.6})$$

Each line of sources then contributes to the voltage  $V$  the amount

$$\varphi - \varphi_o = -\frac{I\rho_s}{2\pi} \ln\left(\frac{e^{\frac{\pi(y_n+s)}{d}} - e^{\frac{-\pi(y_n+s)}{d}}}{e^{\frac{\pi y}{d}} - e^{\frac{-\pi y}{d}}}\right). \quad (\text{V.7})$$

The total voltage between points 1 and 2 is therefore

$$V = \sum \Delta\varphi = -I\rho_s \frac{1}{C\left(\frac{d}{s}\right)}. \quad (\text{V.8})$$

Expanding the logarithm in equation V.4 and summing each term as a geometrical series yields the following equation

$$\rho_s = \Delta\varphi = \frac{V}{I} C\left(\frac{d}{s}\right) \quad (\text{V.9})$$

where  $V$ = voltage,

$I$  = current,

$\rho_s$ = sheet resistivity,

$C$ = a correction factor (depending on the dimension of the sample),

$d$  = width of sample, and

$s$  = probe separation.

With this solution, [35] also stated that it was possible to obtain body resistivity of thin slices of the same finite geometries. The body resistivity of a thin sample can be calculated by multiplying Equation (IV.9) with the thickness ( $w$ ) of the sample.

$$\rho = \rho_s \times w = \frac{V}{I} \frac{d}{s} w. \quad (\text{V.10})$$

Similar to the works of [33] and [34], [35] never assigned a dimension to sheet resistivity or bulk resistivity. It was not until 1962, that bulk resistivity was defined as ohm-cm [36]. However, there was no mention of ohms per square or surface resistivity. In 1968, the term “sheet resistance,” to define thin film resistor parameters was introduced [36]. Reference [36] also reported that the term “number of squares,” was considered a pure number with no dimensions. The sheet resistance has the unit of ohms, but it is convenient to refer to it as “ohms per square.” The concept can be broadened to include any arbitrarily shaped resistor. Reference [36] also stated that the four-point probe is a useful tool to check the uniformity of thin-film resistors.

Due to the confusion caused by the naming convention and dimensions used in resistivity measurements, it is necessary to thoroughly describe the measurement method used in this research. In addition, a complete description of the experimental set-up and material being tested is also required to alleviate any confusion. The next several sections will discuss the method used to conduct bulk resistivity measurements, the experimental set-up and procedures.

### **5.3.2 Four-wire Kelvin Method**

Bulk resistivity measurements for this research were taken using a four-wire “Kelvin” method as per IEEE 1650. Resistance measurements and I-V curve are often made using the two-wire method shown in Figure 14. The test current is sourced through the test leads and the device under test (DUT) resistance being measured. The meter then

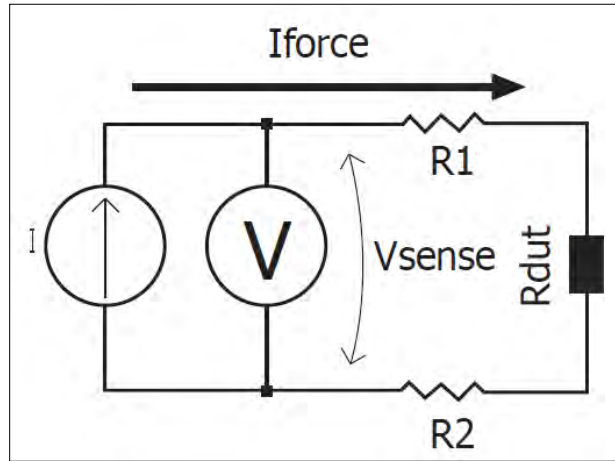


**Figure 14. The Two Wire Resistance measurement [40].**

measures the voltage across the DUT resistance through the same set of test leads and computes the resistance value [38].

The main problem applying the two-wire method for low resistance measurements is that the total lead resistance and contact resistance is added to the measurement [39]. Equations VI.11 thru VI.13 show how resistance can be calculated using Ohm's law.

$$R1 = R_{lead1} + R_{contact1} \quad (V.11)$$

$$R2 = R_{lead2} + R_{contact2} \quad (V.12)$$

$$Vsense = I \times (R1 + R2 + Rdut) \quad (V.13)$$

Test current can cause a significant voltage drop across the lead resistances. As a result the voltage measured by the meter will not be exactly the same as the voltage directly across the test resistance, and considerable error can result. Lead can be, 1 mΩ to 10 mΩ, so it is difficult to obtain accurate two wire resistance measurements when the resistance under test is lower than 10 Ω to 100 Ω [39]. The lead resistance would create

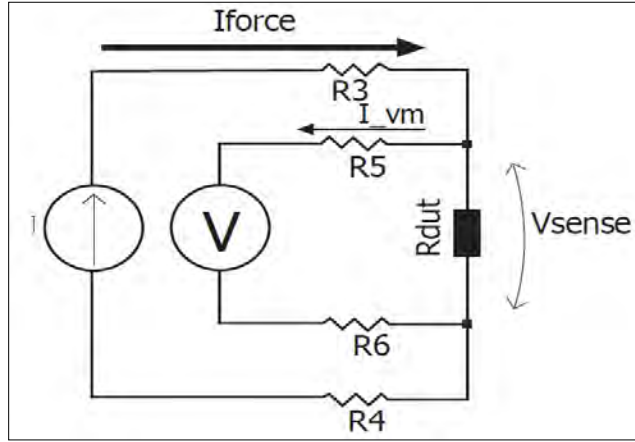


**Figure 15. The Four-Wire Resistance Measurements [40].**

up to a 10% error. Measurements using the two probe method yielded resistivity values ranging from  $3.39 \, \Omega \, \text{cm}$  to  $6.78 \, \Omega \, \text{cm}$  for the MWCNT composites. Measurements using the four probe method yielded resistivity values ranging from  $0.0014 \, \Omega \, \text{cm}$  to  $0.0022 \, \Omega \, \text{cm}$ . The resistivity measurements from the two probe method were three orders of magnitude higher than the four probe method.

Due to the limitations of the two-wire method, the four-wire Kelvin connection method shown in Figure 15 is used for low resistance measurements. In this configuration, the test current is forced through one set of test leads, while the voltage across the DUT is measured through a second set of leads.

$$R3 = R_{lead3} + R_{contact3} \quad (\text{V.14})$$

$$R2 = R_{lead4} + R_{contact4} \quad (\text{V.15})$$

$$V_{sense} = V_{R5} + I \times R_{dut} + V_{R6} \quad (\text{V.16})$$

Therefore,  $I_{vm} = 0$  and  $V_{meas} = I \times R_{dut}$ . A small current may flow through the sense leads. However, it is usually minor and can be ignored [39]. The voltage drop across the sense leads is small, so the voltage measured by the meter is the same as the

voltage across the test resistance. Consequently, the resistance value can be determined much more accurately than with the two-wire method. The voltage-sensing leads should be connected as close to the resistor under test as possible to avoid including the resistance of the test leads in the measurement [39].

#### 5.4 Thermoelectric EMFs Compensation Methods

Thermoelectric EMFs, Johnson noise, magnetic fields and ground loops can produce significant error in low resistivity measurements [39]. The noise voltage is given by

$$V_{EMF} = \sqrt{4kTBR} \quad (\text{V.17})$$

where:  $k$  = Boltzmann's constant,

$T$  = temperature in Kelvin,

$R$  = resistance in  $\Omega$ , and

$B$  = the noise bandwidth in Hz.

Reducing the temperature, resistance, or noise bandwidth will reduce the overall circuit noise. The thermoelectric EMFs can be canceled by making two measurements with currents of opposite polarity. A positive current applied will have a measured voltage of

$$V_+ = V_{EMF} + IR. \quad (\text{V.18})$$

Reversing the current polarity yields the following voltage measurement:

$$V_- = V_{EMF} - IR. \quad (\text{V.19})$$

The two measurements can then be combined to cancel thermoelectric EMFs:

$$V = \frac{V_+ - V_-}{2} = \frac{(V_{EMF} + IR) - (V_{EMF} - IR)}{2}. \quad (\text{V.20})$$

The measured resistance can then be calculated using Ohm's law;

$$R = \frac{V}{I}. \quad (\text{V.21})$$

### 5.5 Resistivity of Bulk Materials (Volume Resistivity)

In order to eliminate lead and contact resistance in the bulk resistivity measurement, the four-wire "Kelvin" method was used in this research. A method for testing the resistivity of a bulk material such as a bar or a rod is shown in Figure 17. The current source is connected to both ends of the sample. The voltmeter leads are placed a known distance apart. The resistivity is calculated from the cross-sectional area of the sample and the distance between the voltmeter leads:

$$\rho = \left(\frac{V}{I}\right) \left(\frac{wt}{L}\right) \quad (\text{V.22})$$

where:  $\rho$  = resistivity in ohm-cm,

$V$  = voltage measured by voltmeter,

$I$  = source current,

$t$  = thickness of sample,

$w$  = width of sample,

$L$  = length between probe in cm,

The inverse of the resistivity is conductivity. Conductivity in units of Siemens/cm can be calculated using Equation VI.23.

$$\sigma = \left(\frac{1}{\rho}\right) \quad (\text{V.23})$$



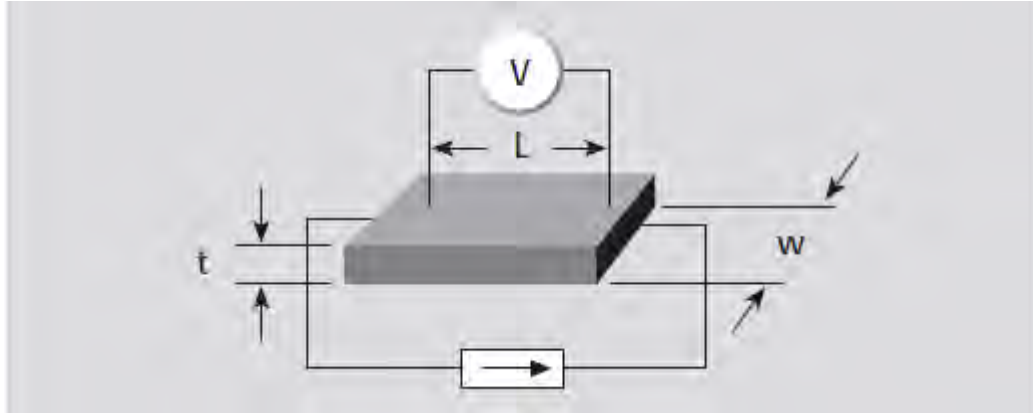


**Figure 16. The Four-Wire Resistance Measurements [40].**

## 5.6 Experimental Set-Up

Figure 17 is a picture of the experimental setup. Four 7078-TRX-10 low noise triax cables connected the Keithley 4200 Semiconductor Characterization System (SCS) to an aluminum enclosure containing the high density polyurethane (HDPE) fixture. The HDPE fixture was secured to the aluminum enclosure with two bolts. The HDPE fixture contained four evenly spaced gold probes which were soldered to four triaxial connectors. Probe 1, 2, and 3 were connected to the Keithley's three source measurement units (SMUs) while Probe 4 was connected to the Keithley's ground unit (GNDU).

## 5.7 Resistivity Measurement Procedure

Following the procedure reported in [1] and [3], resistivity measurements were performed as follows. The sample was first thoroughly cleaned using isopropyl alcohol and then allowed to dry. Next, the first sample was placed flat and centered on the four probes ensuring it did not make contact with either of the two bolts along the sides. The sample was kept in place by securing a second HDPE fixture on top with two finger-tight

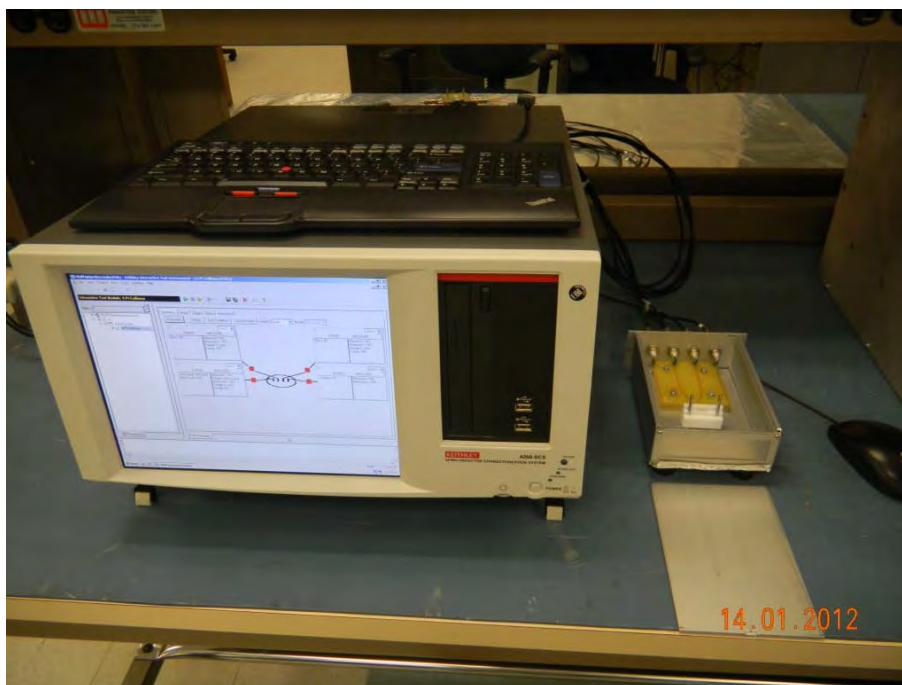


**Figure 17. Bulk resistivity measurement setup. Keithley 4200 SCS on the left and sample holder on the right.**

retaining nuts. Figure 18 is a close-up picture of the test fixture. In order to reduce electromagnetic interference, an aluminum cover was used. Measurements were taken by sourcing current through probe 1 and measuring the voltage drop between probes 2 and 3. The current was stepped from -10 to +10 mA and held for 3 seconds at each step to reduce transient effects. As discussed in Section 5.4, the measurement was taken with alternating current polarity in order to reduce thermoelectric EMF. With the current across the sample known, the voltage drop across probes 2 and 3 was measured and the resistance determined from Ohm's Law as shown in Equation VI.21. The IV data were plotted, where current is plotted along the x-axis and the voltage drop between probes 2 and 3 is plotted along the y-axis. The slope of the regression line was recorded as the average resistance measurement of the sample. Equation VI.22 was then used to find the

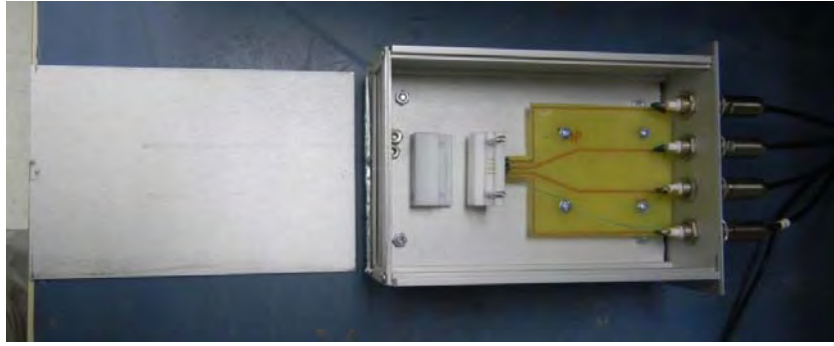


**Figure 18. Resistivity test fixture used to mount samples.**

resistivity of the sample. The conductivity was calculated using Equation VI.23. The sample was removed from the holder and measurement for the second sample was taken following the same procedure as above. This process was repeated for all four samples.

Additional measurements were taken for each sample to determine a distribution associated with that measurement and to determine the 68% confidence interval for each measurement [1], [3]. A total of thirty measurements were taken for each of the samples. However, taking 120 measurements manually also led to several issues. After the first set of measurements, the gold probes had to be replaced and re-soldered to the tri-axial connectors. A second set of measurements were taken which measured a change in the standard deviation for each of the samples. Following vacuum and irradiation, conductivity measurements were repeated as described above. The time it took to conduct the measurement also introduced additional error post-irradiation and post-vacuum. On average, 120 measurements took 6 hours to complete. The samples were exposed to the atmosphere and allowed to anneal for six hours in-between the first measurement and the last measurement. The length of time it took to make the measurements made it difficult to accounting for changes to the electrical property due to

re-absorption of gas and annealing. In addition, finger tight on the first measurement was not the same as figure tight on the last measurement.

Several factors were noted while taking the conductivity measurements that affect measurement precision and repeatability. This is a result of the fabrication process resulting in slightly different surface texture and MWCNT quantities on each face of the panel. As mentioned in Section V, the resistivity measurement technique can be used to test the uniformity of the material. Initial measurements indicated that the samples were not uniform. In order to increase the repeatability and precision of the measurement, the sample was always placed in the same orientation. A red mark was made on the side of each sample and the samples were always placed in the holder with the red dot on the right hand side facing toward the inside of the holder.

Additional measurements were used for comparison to the primary measurements described previously. This was first conducted by placing the sample in the holder as far to one side as possible, so as to contact the bolt on that side. This method was not desired due to the potential for the bolt to provide an alternate conductive path to the outside, thus negating the purpose of the aluminum box. In addition, the placement caused an uneven contact between the sample and the four probes. The displaced sample had 18 % larger resistivity than the centered sample. This indicated that the contact with the side bolts provided an alternate conductive path to ground. As a result, a larger voltage drop between probes two and three was measured. According to Equation V.22, the increase in voltage drop would increase the resistivity measurement. Placing the sample in the center of the fixture prevented this error in the resistivity measurement.



**Figure 19. Copper samples used to verify surface conductivity measurements.**

A second additional test was conducted using three different copper samples. Each copper sample was cut from three different gaskets with different dimensions. The copper samples, Figure 19, had a smoother surface and were more uniformed than the MWCNT composite sample and were therefore expected to show smaller standard deviation in the measurement values. The average bulk resistivity for the copper samples is listed in Table 3. The accepted value for surface resistivity of copper is  $1.68 \times 10^{-6} \Omega \text{ cm}$ , as listed in [37]. The measurements indicated that the test fixture was appropriate for measuring low resistance material. The difference in the measured resistivity was due to the thickness of the copper sample. The thinner the sample, the closer the bulk resistivity was to the accepted value for surface resistivity.

**Table 3. Resistivity of the three copper samples**

Copper	Width (cm)	Thickness (cm)	Mean Resistivity ( $\Omega \text{ cm}$ )	Standard Deviation (+/-)
1	0.2855	0.2011	$9.36 \times 10^{-6}$	$2.0 \times 10^{-8}$
2	0.2251	0.0627	$1.58 \times 10^{-6}$	$1.8 \times 10^{-8}$
3	0.3000	0.0534	$1.61 \times 10^{-6}$	$1.0 \times 10^{-8}$

## 5.8 EMI Shielding Effectiveness Theory

This section will address the concept and theoretical development of EMI shielding effectiveness. The analysis of electromagnetic shielding effectiveness should begin with the quantum theory of materials. However, for the purpose of this research, the classical electromagnetism will be used as the theoretical basis. The concept of shielding refers to a metallic enclosure that completely surrounds an electronic device that either radiates or is susceptible to electromagnetic interference. The shield serves two purposes: to exclude EMI from disrupting normal functions of internal electronics, and to prevent radiated emissions from interfering with external electronic components. Only EMI-SE against an external source will be examined.

### 5.8.1 Theoretical Consideration

The mechanisms through which power is lost through the shielding materials are quantum in nature (i.e., on the atomic and crystal lattice levels). In order to understand the influence of each shielding mechanism on the overall EMI-SE of a MWCNT composite, a model quantifying the EMI-SE of a homogenous conductive plate attenuating the EM far-field radiation will be discussed. For far-field radiation, the incident field impinging on the shield will resemble a uniform plane wave. When an electromagnetic plane wave is incident on a solid conductive material having different intrinsic impedance than the domain in which the EM plane wave was traveling, two waves will be created at the interface: a reflected wave ( $E_R$ ) and a transmitted wave ( $E_T$ ) through the barrier. Figure 20 depicts this process.

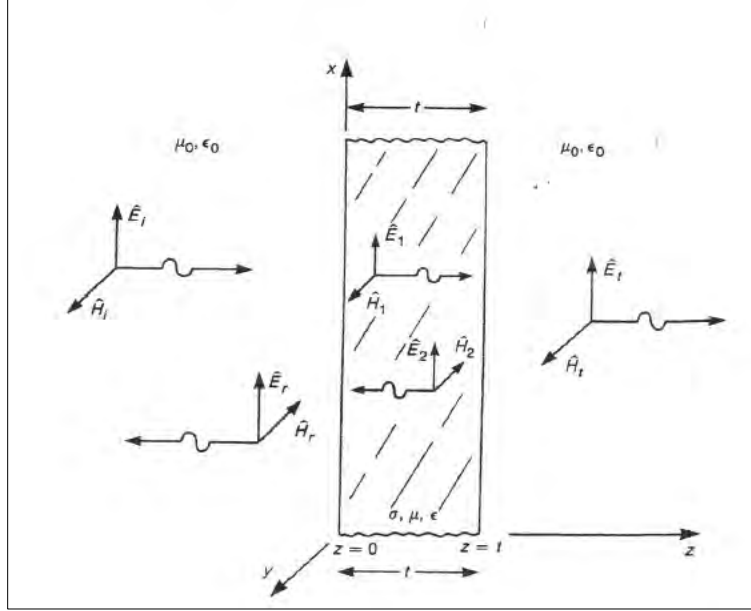


**Figure 20. Electromagnetic wave propagating through a solid conductive material [6].**

The total shielding effectiveness of the barrier is then defined in decibels as

$$SE = 20 \log_{10} \left| \frac{E_t}{E_i} \right| \quad (V.24)$$

where  $E_t$  is the transmitted wave and  $E_i$  is the incident wave. In this form of the equation, the  $SE$  will be negative.

There are several phenomena that contribute to the reduction of the incident field passing through the barrier. Figure 20 shows some of these phenomena. The first is reflection at the near side surface of the barrier. The portion of the wave that crosses this surface proceeds through the shield wall. As it passes through this conductive medium, its amplitude is attenuated according to the factor  $e^{-t/\delta}$ , where  $t$  is the thickness of the barrier and  $\delta$  is the skin depth of the barrier material. The skin depth is the distance it takes to reduce the amplitude of the incident field by a factor of  $1/e$ . Increasing shield

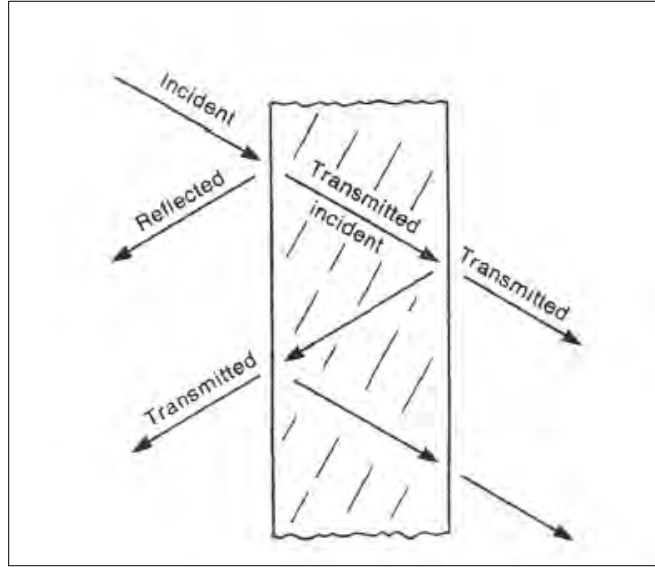


**Figure 21. Multiple internal reflections.**

conductivity, magnetic permeability and EM wave frequency will decrease the skin depth.

The skin depth ( $\delta$ ), can be approximately calculated using

$$\delta = \sqrt{\frac{2}{\omega\mu\sigma}} \quad (\text{V.25})$$

where

$\mu$  = magnetic permeability of the material,

$\sigma$  = the conductivity of the material, and

$\omega$  = the frequency of incident wave.

The total shielding effectiveness is broken down into reflection loss, absorption loss, and multiple reflections. These factors are given in decibel in Equation VI.26.

$$SE_{dB} = R_{dB} + A_{dB} + M_{dB} \quad (\text{V.26})$$

The loss due to reflection is



$$R_{dB} = 20 \log_{10} \left| \frac{\eta_o}{4\eta_m} \right| \quad (\text{V.27})$$

where  $\eta_o$  is the intrinsic impedance in free space and  $\eta_m$  is the intrinsic impedance of the conductor. For electromagnetic plane wave in free space, the conductivity ( $\sigma$ ) is equal to zero. Therefore,  $\eta_o = \sqrt{\mu_o/\epsilon_o}$  where  $\mu_o$  and  $\epsilon_o$  are the permeability and permittivity of free space. For conductive materials,  $\sigma \gg \omega\epsilon$ , yields

$$\eta_m = \left| \frac{E}{H} \right| = \sqrt{\frac{j\omega\mu}{\sigma + j\omega\epsilon}} = \sqrt{\frac{j\omega\mu}{\sigma}}. \quad (\text{V.28})$$

Assuming  $\mu = \mu_o \mu_r$  and  $\epsilon = \epsilon_o$ , Equation V.27 can then be rewritten as

$$R_{dB} = 20 \log_{10} \left( \frac{1}{4} \sqrt{\frac{\sigma}{\omega\mu_r\epsilon_o}} \right) \quad (\text{V.29})$$

The loss due to absorption is

$$A_{dB} = -20 \log_{10} \left| e^{\frac{t}{\delta}} \right| \quad (\text{V.30})$$

The loss due to multiple-reflection

$$M_{dB} = -20 \log_{10} \left| 1 - e^{\frac{t}{\delta}} \right| \quad (\text{V.31})$$

According to Equation V.30, The amount of energy absorbed increases with an increase in the shield thickness and decrease in skin depth. If the thickness of the shield is much greater than the skin depth of the barrier at the frequency of the incident wave, the wave is greatly attenuated as it travels through the barrier before it strikes the far side interface. The reflected portion of this wave is transmitted back through the barrier and strikes the near side interface. Portions of the wave transmitted through the right interface add to the total field that is transmitted through the entire shield. The reflected and

transmitted fields are progressively attenuated by their travel through the conductive barrier. According to Equation VI.31, if the thickness of the shield is much greater than the skin depth, the multiple reflection and transmission can be disregarded because  $M_{dB}$  will be a relatively small number. However, if the thickness of the shield is smaller than the skin depth, the  $M_{dB}$  significantly decrease the total EMI-SE. Table 4 is an example of how skin depths can affect the overall EMI-SE of copper. The skin depth at frequency of 8.4 GHz, relative permeability and relative conductivity for copper was used to calculate the values in Table 4.

**Table 4. The effects of skin depths on overall EMI-SE.**

	Skin Depths(m)	Thickness of Shield (m)	$R_{dB}$	$A_{dB}$	$M_{dB}$	$SE_{dB}$
Thick Shield	$6.15 \times 10^{-6}$	.00001	-111	-14	-0.34	-125
Thin Shield	$6.15 \times 10^{-6}$	$1 \times 10^{-8}$	-111	-.001	69	-45

## 5.9 Measurement Technique

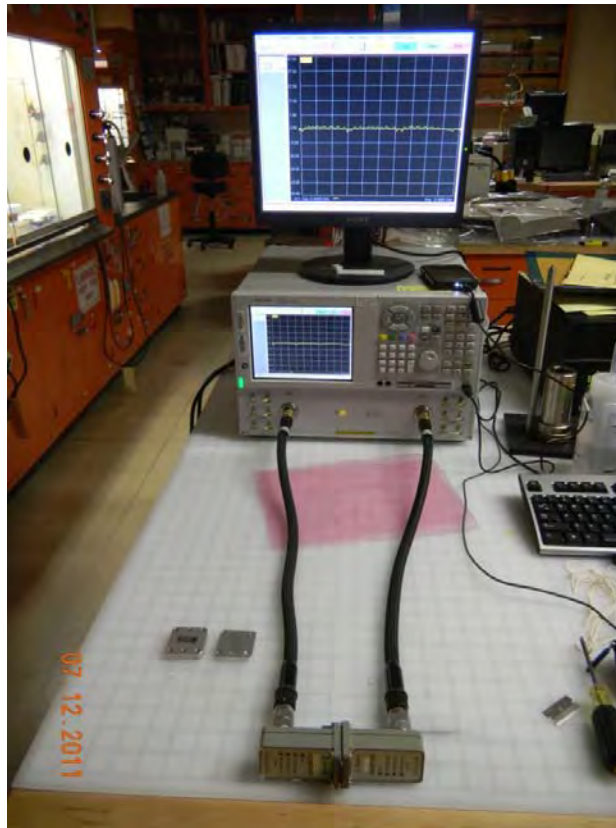


**Figure 22. Network Analyzer used to measure EMI-SE.**

**Figure 22 is the EMI-SE measurement set-up. All EMI-SE tests were performed at the AFRL Materials and Manufacturing Directorate (AFRL/RX) at room temperature and pressure. EMI measurements were conducted with the Agilent Technologies E8362B PNA Series Network Analyzer before and after vacuum and irradiation. The network analyzer is a common tool used to measure the shielding effectiveness of materials. The instrument compares an unknown signal with a reference signal of the same frequency. The impedance of the input line has been carefully designed to “match” the impedance of the source, and the impedance of the output line is matched to the impedance of the load or detector terminating the output of the device. The network analyzer maintains these conditions for test frequencies of 8.2 GHz to 12.4 GHz (X-Band) when the test sample is being measured. Calibration procedures were performed prior to conducting each EMI-SE measurements on the network analyzer.**

Appendix A outlines the calibration steps performed and they were necessary to collect accurate data for the frequency range of 8.2 GHz– 12.4 GHz. The purpose of the

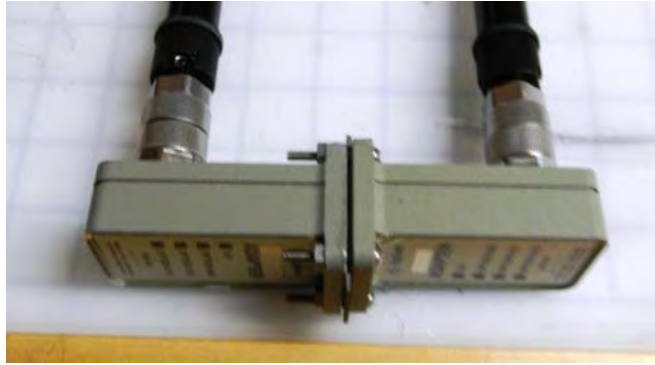


**Figure 23. Sample holder for EMI-SE measurement.**

calibration is to determine several undesired parameters that may be removed or suppressed from the test sample data by subsequent mathematical operations [41].

#### **5.10 EMI-SE Measurement Procedure**

The samples were first thoroughly cleaned using isopropyl alcohol and allowed to dry. EMI-SE measurements were taken at the same locations for each specimen, with 201 continuous sweep points, and auto-correction selected on the network analyzer. Figure 23 illustrates how each specimen was secured horizontally between the adapters for measurements. A red waxed pencil was used to mark the side of each sample to ensure measurements were taken at the same location. A second set of red marks was used to ensure electrons from the irradiation fell on the same measured location.

Several factors were noted while taking the EMI-SE measurements that affect measurement precision and repeatability. A modified mounting method was used to take the EMI-SE measurement. The sample panels had to be a certain dimension in order to be used for follow on mechanical stress experiments. As a result, the panels did not fit the network analyzer ports correctly. The samples protruded from the side of the ports as shown in Figure 23. In addition, the modified setup made it difficult to mount the sample

the same way for each measurement. How tightly the panels were held together between the ports with the four mounting screws also affected the EMI-SE measurements. The modified setup introduced additional error in the EMI-SE measurements. In order account for the variation in the measurement caused by the modified set-up, the samples were removed in between each measurement. A total of thirty measurements were taken for each of the four samples.

## VI. Sample Irradiation

### 6.1 Overview

Electron irradiation was conducted at Wright State University's Dynamitron facility. The 1.6-MeV Dynamitron accelerator boils electrons from a hot filament and accelerates them with a voltage drop of up to 1.6 million volts. These electrons can then be made to impinge on targets for purposes of analysis or radiation damage. The electrons exiting the accelerator and pass through an evacuated beam line to the sample chamber. The samples are mounted in the sample chamber on a cold head that is used to keep sample heating to a minimum. The cold head is electrically isolated from the rest of the beam line and is connected to a current integrator on the main control rack for the purposes of determining electron fluence.

Pre-irradiation calculations were conducted to verify the appropriateness of the energy range and to ensure the correct fluence would be applied for each irradiation. Average electron energy of 0.5 MeV was chosen for comparison with previous work and based on results from CASINO<sup>®</sup> electron simulation. The results from the simulation indicated that the most energy was deposited within the MWCNT composite using 0.5 MeV electrons. The mass of the samples was measured and the density calculated using the dimension of the panels. An average density of 2.62 grams/cm<sup>3</sup> for the MWCNT composite layer was used for the CASINO<sup>®</sup> electron simulation.

In addition, the sample is held in a vacuum of 10<sup>-6</sup> Torr during electron irradiation. To determine if any observed changes in conductivity or EMI-SE could be attributed to out-gassing, a vacuum check was conducted. All of the samples were placed

in the sample chamber and exposed to a vacuum of  $10^{-6}$  Torr for approximately 24 hours. The sample were then removed and EMI-SE and conductivity measurements taken. A detailed discussion and analysis of the result will be presented in Chapter VII.

## 6.2 Dynamitron Electron Irradiation

The primary instrument readouts used when operating the Dynamitron Electron Accelerator are electron energy, beam current and total Coulomb count. As discussed previously the electron energy used for initial irradiations was 0.5 MeV. The beam current used was 6  $\mu$ A and the charge count varied with desired fluence level. The coulomb count was determined according to Equation VI.1 to ensure the correct electron fluence was achieved.

$$Count = \frac{Desired\ Fluence \times Charge\ per\ Electron \times Beam\ Area}{Full\ Scale\ Factor} \quad (VI.1)$$

The charge per electron is  $1.602 \times 10^{19}$  C, the beam area was 2.74 cm in diameter and the full scale factor was 6  $\mu$ A. Through the use of Equation VI.1 and using the recorded parameters, a coulomb count of 1572 was desired to achieve a fluence of  $10^{16}$  electrons/ $cm^2$ .

Figure 24 depicts the mounting method used for the MWCNT composite samples. Two sided scotch tape was used to ensure the samples were secured to the cold head. The cold head was then attached to the end of the beam line and electrically isolated. In order to prevent any thermal damage from the electron beam, water was used to cool the cold head and ensure the samples were maintained at room temperature. The beam line was placed under vacuum to a level of  $10^{-6}$  Torr.

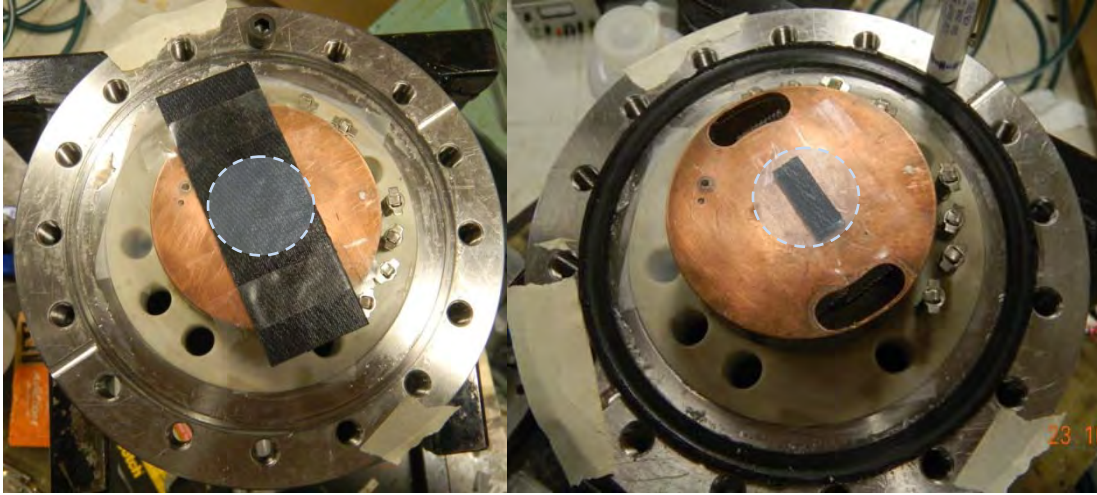


**Figure 24. Samples mounted on the cold head. Sample for EMI-SE on the left and samples for resistivity measurements on the right. The blue circle indicates the electron beam spot.**

After the first electron irradiation, the sample was removed from the cold head and post irradiation resistivity measurements and EMI-SE measurements were taken approximately 1 hour post irradiation. Table 5 summarizes the operating parameters for each irradiation. Parameters for Irradiation #1 was the same for all MWCNT composites sample configuration. Parameters for Irradiation #2 thru #4 were used for 3 different samples of 2CNT/4GL/2CNT to investigate the possibility of transient ionizing radiation effects on the MWCNT composites.

**Table 5. Electron irradiation operating parameters**

	Electron Energy (keV)	Fluence (e/cm <sup>2</sup> )	Coulomb Count [C]	F.S. Factor [μA]	Vacuum [Torr]
Irradiation #1	500	$1 \times 10^{16}$	1572	6	$10^{-6}$
Irradiation #2	100	$3.75 \times 10^{16}$	1572	2	$10^{-6}$
Irradiation #3	200	$1 \times 10^{16}$	1572	6	$10^{-6}$
Irradiation #4	500	$1 \times 10^{16}$	1572	6	$10^{-6}$



### 6.3 Neutron Irradiation

Neutron irradiation was conducted at the Ohio State University Research Reactor (OSURR). The OSURR is a uranium reactor surrounded by a 20 foot deep pool of water. The pool provides cooling, neutron moderation, and gamma shielding. A vertical irradiation chamber was used for these experiments. The irradiation chamber consists of a 20.5' long, 7" outside diameter aluminum tube (6061 T6 aluminum) with walls 0.125" thick. The chamber was moved into contact with the reactor with the top of the chamber tube against a bracket during each experiment. The chamber allowed access to the high neutron flux position adjacent to the reactor core while allowing easy access for the samples and mounting apparatus. The basic configuration is shown Figure 25. The reactor can operate continuously at full power up to a maximum of 500 kW. The average thermal neutron flux in the core is approximately  $5 \times 10^{12}$  neutrons/cm<sup>2</sup> s. The samples were placed in a cadmium box in order to shield from thermal neutrons. The cross section is 5 orders of magnitude greater for neutron absorption in cadmium compared to carbon at energies below approximately 0.45 eV. Therefore in the 1 MeV equivalent calculations we assumed that neutrons below 0.45 eV are absorbed by cadmium. Neutrons of energy greater than 1.5 eV pass through cadmium with little attenuation.

Equation IV-1 was used for the 1 MeV equivalent mono-energetic neutron fluence conversions in the 7 inch dry tube.  $E_{\max}$  and  $E_{\min}$  were set at 1.8 MeV and 0.5 eV upper and lower limits in the integral in Equation IV.1.  $F_{D,Mat}$  for each energy is found in table A1.1 of ASTM E722. The values in table A1.1 were multiplied by  $3.45 \times 10^{-13}$  to convert to rad (Si)-cm<sup>2</sup>.  $F_{D,1MeV,Mat}$  is given in ASTM E722 as 95 MeV-mb. Simpson's

rule was then used to carry out the integral in Equation VI.1. The resulting 1 MeV (eq) neutron flux in the 7 inch dry tube beam port is equal to  $10^{11}$  neutrons/cm<sup>2</sup> for a power setting of 450 kW. Using the desired neutron fluence and the neutron flux the total amount of time of irradiation was determined to be 16 minutes and 40 seconds achieve a total fluence of  $10^{11}$  neutrons/cm<sup>2</sup> s. However, since the samples were exposed to neutrons as the reactor is powered up and powered down, a lower power and longer irradiation time is desired. Running the reactor at a lower power reduced the flux and a longer irradiation time was necessary in order to irradiate the sample to the same fluence. This was done by taking the 1 MeV (eq) neutron flux at 450 kW and scaling to the 1 MeV (eq) neutron flux at 100 keV. The 1 MeV (eq) neutron flux at 100 keV was  $6.67 \times 10^{10}$  neutrons/cm<sup>2</sup> s. To achieve a fluence of  $10^{14}$  neutrons/cm<sup>2</sup> the reactor was operated for 75 minutes. Table 6 contains the parameter used in the irradiation.

**Table 6. OSURR irradiation setting**

	Fluence Neutrons/cm <sup>2</sup>	Flux Neutrons/cm <sup>2</sup> s	Reactor Power (kW)	Irradiation Time (minutes)
Initial Setting	$1.0 \times 10^{14}$ neutrons/cm <sup>2</sup>	$1.0 \times 10^{11}$	450	17
Irradiation #1	$1.0 \times 10^{14}$ neutrons/cm <sup>2</sup>	$2.2 \times 10^{10}$	100	75
Irradiation #2	$1.0 \times 10^{14}$ neutrons/cm <sup>2</sup>	$6.7 \times 10^{10}$	300	250

A LEO satellite experiences a fluence of  $10^{16}$  protons/cm<sup>2</sup> during its 35 year life cycle. The first step to find the neutron NIEL equivalent is to find the NIEL rate for protons. This is accomplished using figure 3.24 in [27]. It is important to note that the conversion factors were created for silicon. Applying this chart to our MWCNT

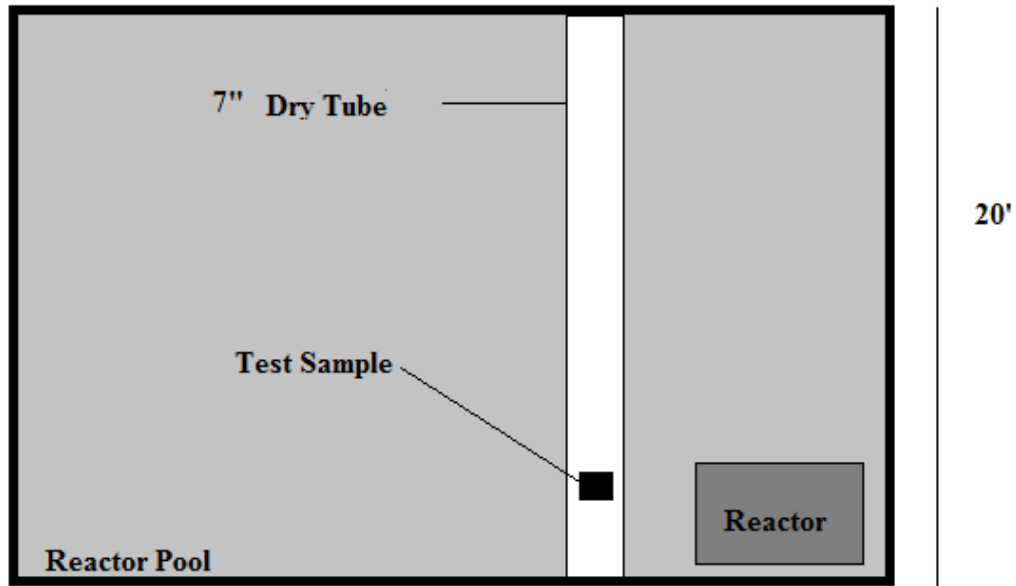


**Figure 25. Ohio State University Research reactor.**

composites introduces error in our calculations. The NIEL rate for protons is 50 keV cm<sup>2</sup>/g. The proton NIEL rate multiply by the proton fluence yields  $5.52 \times 10^{17}$  keV proton/g. To calculate the neutron equivalent NIEL, the proton NIEL is divided by the neutron NIEL. This is equal to a fluence value of  $5.02 \times 10^{19}$  neutrons/cm<sup>2</sup>. However, for comparative purpose, the same fluence levels for irradiation were used as [1]. The samples were irradiated with 1MeV (eq) neutrons to fluence levels of  $10^{14}$  neutrons/cm<sup>2</sup> and  $10^{15}$  neutrons/cm<sup>2</sup>.

## **VII. Results and Analysis**

### **7.1 CASINO<sup>®</sup> Simulation Results**

The CASINO<sup>®</sup> electron simulation code was used to predict the suitability of the energy range applied for each irradiation. The results are depicted in Figure 26 through Figure 27. The three figures show the penetration depth of electrons in the different test sample configurations. The stopping point for the simulated electrons and most of the electron energy is predicted to be deposited in the final 10% of the electron's range. The energy distribution would be spread-out slightly to the left of the penetration depth.

For 1.0 MeV electrons, the majority of the electrons are deposited in the cold-head of the Dynamitron as shown in Figure 26. Figure 27 shows results for 500 keV electrons on the four different samples. The majority of the electrons deposited their energy in the samples. However, it is difficult to determine whether the energy was deposited in the SiO<sub>2</sub> glass layer or the MWCNT composite layer. Figure 28 shows the penetration depth of 100 keV and 200 keV electrons. For lower energy level, most of the electron energy was deposited in the first two layers of the MWCNT composite. The three simulation results confirmed the best selections for electron energy are between 100 keV and 500 keV.

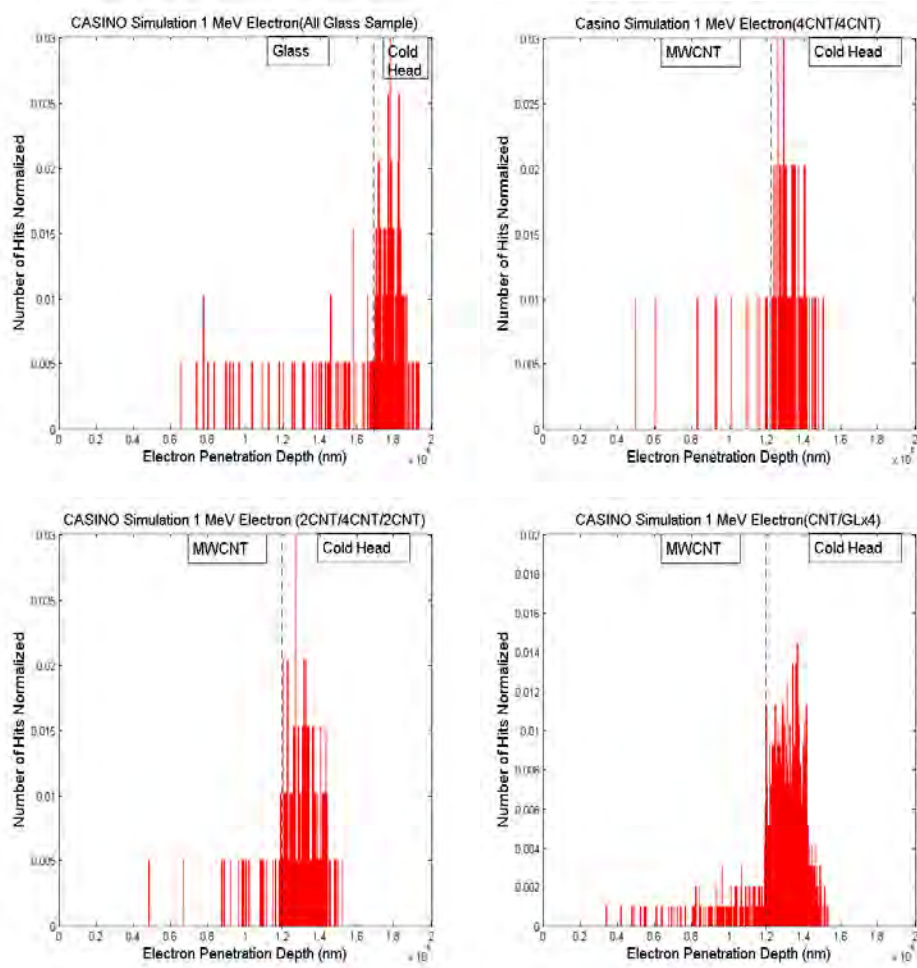


**Figure 26. Results of CASINO<sup>®</sup> simulation showing electron penetration depth of 1 MeV electrons. The four separate figures show the four different sample types as noted in the headings. The dash line represents the sample (to the left of the dashed line) and cold-head (to the right) interface.**

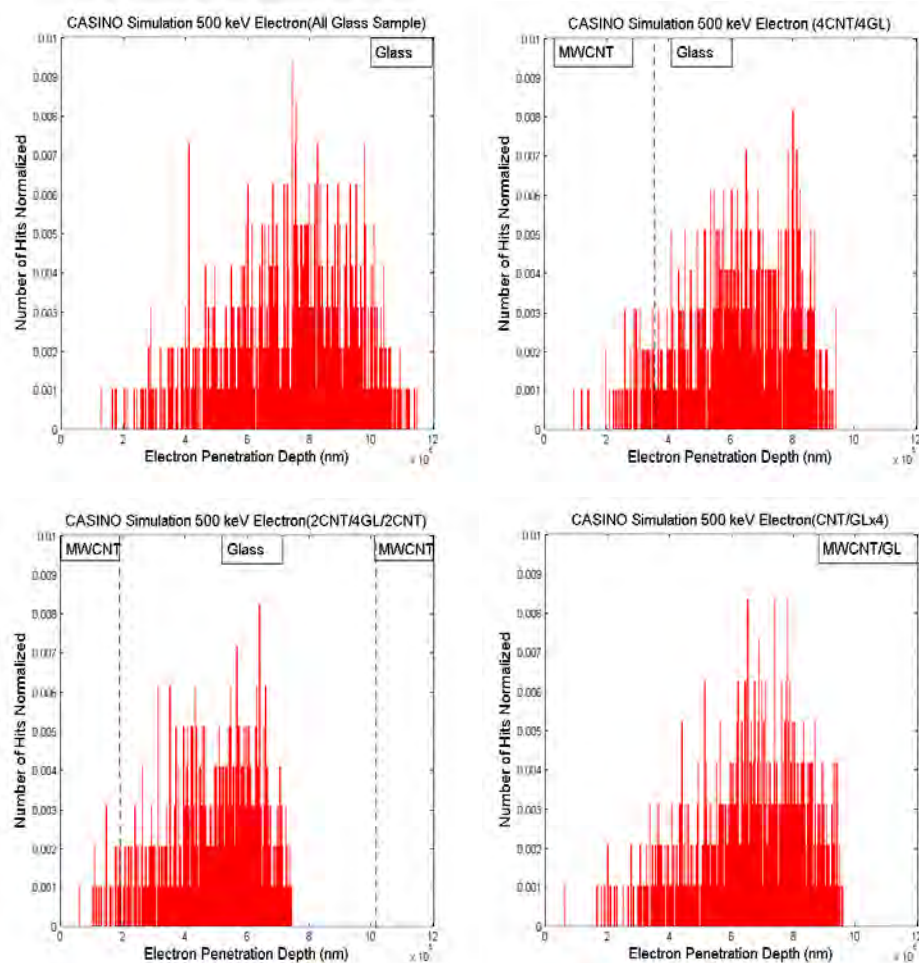


**Figure 27. Results of CASINO<sup>®</sup> simulation showing electron penetration depth of 0.5 MeV electrons. The four separate figures show the four different sample types as noted in the headings. The dash line represents the MWCNT (to the left of the dashed line) and SiO<sub>2</sub> (to the right) interface.**

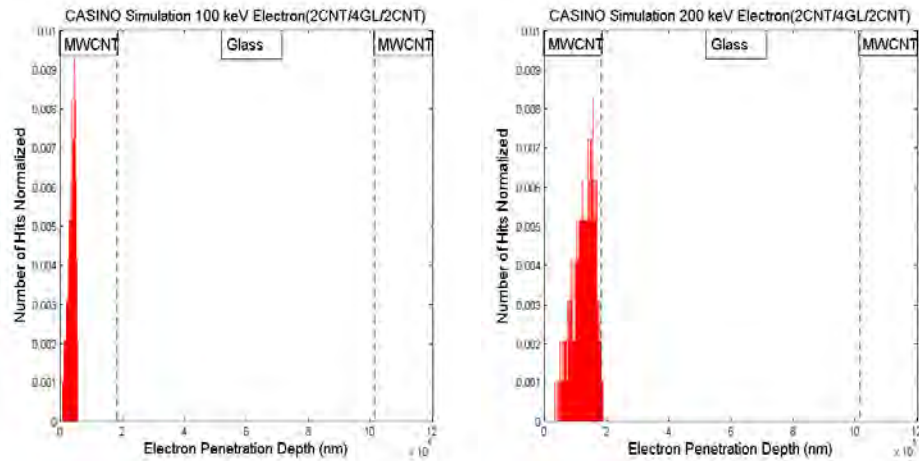


**Figure 28. Results of CASINO® simulation showing electron penetration depth of 0.1 and 0.2 MeV electrons. The 2 separate figures show the same sample as noted in the headings. The dash line represents the MWCNT (to the left of the dashed line) and SiO<sub>2</sub> (to the right) interface.**

## 7.2 Pre-characterization Results and Analysis

### 7.2.1 Initial Conductivity Results and Analysis

Table 7 contains the pre-vacuum and pre-irradiation conductivity of the MWCNT composites. Due to the high resistivity of SiO<sub>2</sub> glass ( $> 10^{16} \Omega \text{ cm}$ ) **Error! Reference source not found.**, measurements could not be taken with the resistivity test fixture. The fixture and test method was specifically designed to measure low resistivity samples. Nevertheless, several attempts were made to measure the resistivity of SiO<sub>2</sub> glass with the test fixture. The values measured ranged from  $1 \Omega \text{ cm}$  to  $10^3 \Omega \text{ cm}$  which were several orders of magnitude from the accepted value for SiO<sub>2</sub>. As mentioned in section 5.7, the test fixture was used to measure the resistivity of copper, a low resistance metal. The fixture was able to accurately measure the resistivity of three different copper samples. The resistivity of

MWCNT composites are not as low as copper. However, they are on the order of  $10^{-3}$   $\Omega$  cm which is only three orders of magnitude higher than copper. On the other hand, the resistivity of SiO<sub>2</sub> glass is more than 12 orders of magnitude greater than that of copper.

**Table 7. Conductivity results from vacuum check ( $10^{-6}$  Torr)**

Mean Conductivity (S/cm)	4CNT/4G	+/- (S/cm)	2CNT/4G/2CNT	+/- (S/cm)	G/CNTx4	+/- (S/cm)
Pre-Vacuum(1)	662	11	455	3	459	12
Pre-Vacuum(2)	685	4	453	58	501	27
Post Vacuum	674	11	451	7	467	15

Table 7 also has two sets of pre-vacuum measurements. A wire connecting a gold probe to the tri-axial connector on the resistivity test fixture broke after the first set of measurements. As a result, all the gold probes were replaced and re-soldered to the wires leading to the tri-axial connectors. The two sets of measurements are shown to illuminate several observation made by [1]. The new probes were in better contact with the test sample. As discussed by [1], the probes were able to push through the epoxy layer and make better contact with conductive pathway of the MWCNTs. There was an increase in the measured conductivity of the 4CNT/4GL and CNT/GLx4 sample between the two pre-vacuum measurements. The increased in conductivity can be attributed to the new gold probes making better contact with the test sample. On the other hand, the conductivity of the 2CNT/4G/2CNT had a slight decrease in conductivity that was within the standard deviation of the first measurement. The standard deviation, however, increased to  $\pm 58$  S/cm. This can be attributed to the unique uneven surface of the 2CNT/4G/2CNT sample. The uneven surface made it difficult to place the sample stick



in the same position for each measurement. As a result, the current took a different path through the conductive layer during each measurement and increase the standard deviation.

### **7.2.2 Initial EMI-SE Results and Analysis**

Figure 29 is the EMI-SE of MWCNT composites prior to vacuum test and irradiation. The thin line is the actual EMI-SE signal of each of the sample panels. The thicker line is a Savitzky-Golay smoothing filter that is commonly used to smooth out noisy digital signals. Pre-characterization results were consistent with the focused beam test results reported by [2]. The focused beam test was performed with a custom made Georgia Tech Research Institute device. The device is capable of measuring EMI-SE between 2GHz -18GHz. EMI-SE measurements were taken with the focused beam using 30.5 cm × 30.5 cm panels of the MWCNT composite. Measurements from the focused beam test were used to validate EMI-SE measurements from the network analyzer.

The control sample containing only SiO<sub>2</sub> glass layers had nearly zero EMI-SE (-0.7dB ± 0.3dB). The 2CNT/4G/2CNT sample had the highest average EMI-SE at -84.37 dB ± 0.01dB and the CNT/GL×4 sample had the lowest EMI-SE at -71.94 dB ± 0.01 dB. The 4CNT/4GL sample had a lower magnitude of EMI-SE than what was measured by the focused beam test. The 4CNT/4GL sample had an EMI-SE of -74.06dB ± 0.01dB as measured by the network analyzer and -87.497 dB as measured by the focused beam test.

All three composite panels had the same 90 %wt of MWCNT and the same relative thickness. However, they did not have the same shielding effectiveness. The 2CNT/4G/2CNT sample had the highest EMI-SE and both the 4CNT/4GL and the CNT/GL×4 sample had roughly the same EMI-SE as measured by the network analyzer.

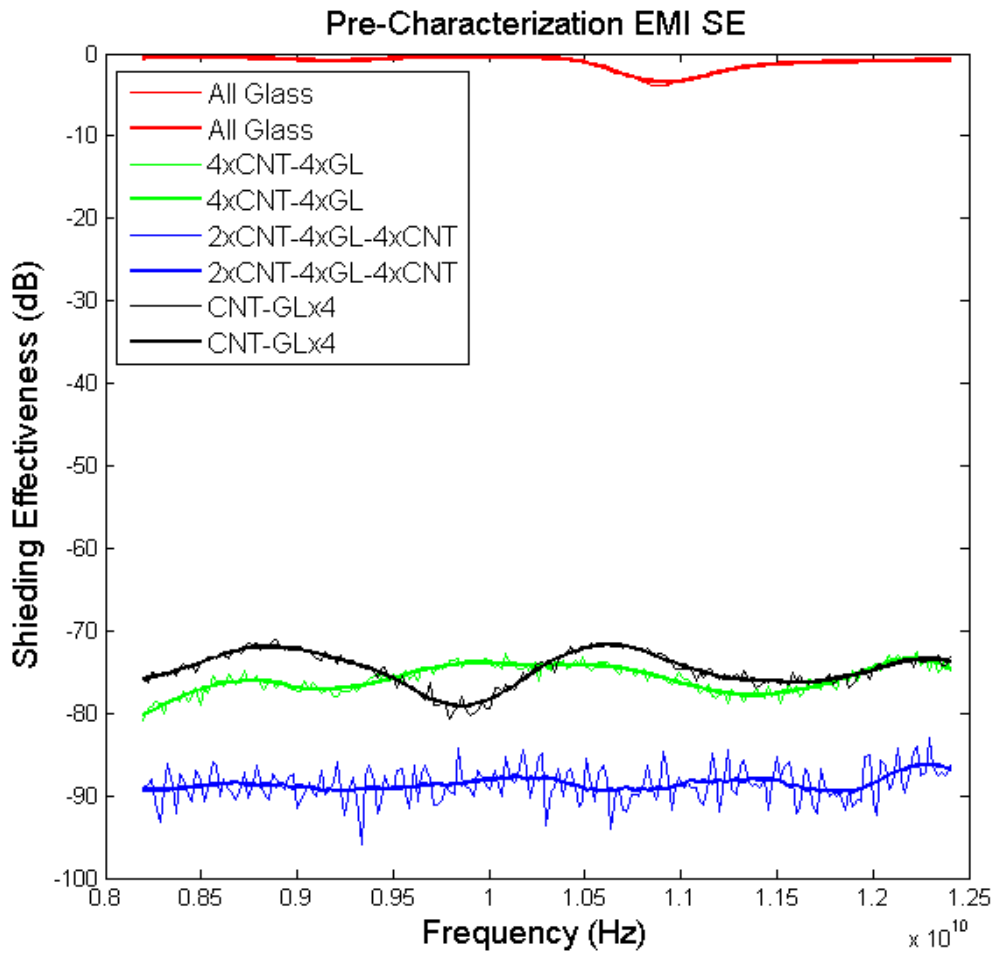


**Figure 29. Pre-characterization of EMI Shielding Effectiveness. The thick line represents a Savitzky-Golay smoothing filter of the EMI signal.**

However, the 4CNT/4GL configuration had a much higher EMI-SE when measured with the focused beam as reported by [2]. The difference in the measured SE may be a result of delamination when the sample was cut from the larger panel that was used for the focus beam test.

The CNT/GL $\times$ 4 had the least EMI-SE even though it had an equal percent weight of MWCNTs and same thickness as the other two panels. This can be explained using the shielding theory as discussed in section 5.8.1. If the thickness of the shield is greater

than the skin then the multiple reflection component of the total SE is negligible. If the thickness of the shield is less than skin depth, then the  $M_{dB}$  component decrease the overall EMI-SE of the composite. However, theoretical calculation indicates that the thickness of the MWCNT layer for all three samples is greater than the skin depth and that multiple internal reflections had negligible effects on the overall EMI-SE. As indicated in Table 8, the primary power loss mechanisms through the MWCNT composite are from reflection and absorption. The theoretical EMI-SE is much higher than the measured experimental value. The differences between the results are due to several factors. Using the thickness of the MWCNT composite instead of the thickness of the carbon nanotube bucky paper resulted in a much higher EMI-SE calculation. In addition, the MWCNTs are hollow structures. Internal reflections within the nanotubes are also not taken into account in the theoretical calculation. A third factor not taken into account is the multiple reflections between the external layers of the MWCNT composite. The three factors resulted in a much higher estimation of the composites' EMI-SE as compared to the experimental value.

**Table 8. Effects of Skin Depths on EMI-SE of MWCNT**

	Freq (Hz)	Skin Depths	Shield (cm)	$R_{dB}$	$A_{dB}$	$M_{dB}$	Theory $SE_{dB}$	Experiment $SE_{dB}$
2CNT/4GL/2CNT	8.4	0.0000257	0.0172	-36	-116	0	-152	-84
4CNT/4GL	8.4	0.0000213	0.0344	-39	-140	0	-179	-74
CNT/GL×4	8.4	0.0000245	0.0086	-36	-116	0	-152	-71

### 7.3 Post Vacuum Result and Analysis

Table 7 contains the conductivity results from the vacuum check. The G/CNT×4 sample had a 6.8% decrease in conductivity. However, the decrease can be attributed to using new probes which caused additional variations in the measurement. The 4CNT/4G and 2CNT/4G/2CNT had a 1.6% and 0.44% change respectively. Figure 30 is the EMI-SE results from the vacuum check. Two vacuum checks were conducted. The first used an external turbo pump that brought the MWCNT composites under vacuum to  $10^{-5}$  Torr for less than 24 hours before malfunctioning. The second vacuum check involved using the Dynamitron. The MWCNT composites were placed in the sample chamber of the Dynamitron and sealed. The air was then evacuated from the beam line. The samples were under a vacuum of  $10^{-6}$  Torr for approximately 24 hours. This is the same vacuum level the sample will experience during the electron irradiation. The samples were then removed from the Dynamitron and EMI-SE measurements were taken. The process was repeated using samples for the resistivity measurements. On average, the measurements were taken approximately 1 hour immediately following the vacuum test. Table 9 contains the average EMI-SE of the MWCNT panels post vacuum. Changes were on the order of the pre-vacuum standard deviation.

**Table 9. EMI-SE Vacuum Test**

	Pre-Vacuum		Vacuum Test 1		Vacuum Test 2	
	Mean EMI-SE (dB)	± (dB)	Mean EMI-SE (dB)	± (dB)	Mean EMI-SE (dB)	± (dB)
8GL	-0.700	0.30	-0.70	0.30	-0.8	0.30
4CNT/4GL	-74.06	0.01	-77.49	0.01	-73.13	0.02
2CNT/4GL/2CNT	-84.37	0.01	-87.23	0.01	-86.05	0.01
CNT/GLx4	-71.94	0.01	-73.01	0.02	-69.29	0.02

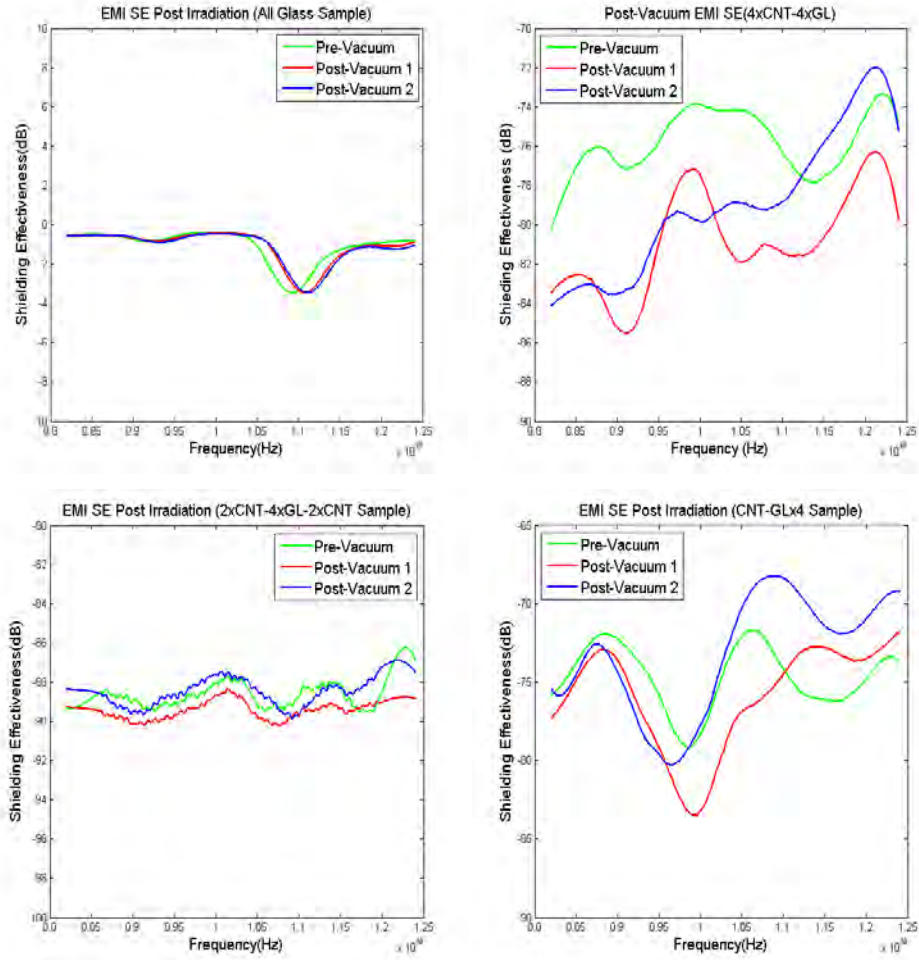


**Figure 30. A comparison of changes to the MWCNT composites post vacuum. The four separate figures show the four different sample types as noted in the headings.**

As discussed in section 3.6, electrical properties of MWCNT can be changed by absorbing gaseous species in the atmosphere. Although the changes to the electrical property of the MWCNT composites were insignificant, for future research consideration and thoroughness, an analysis of the vacuum effects are presented. The 4CNT/4GL and the CNT/GLx4 sample both had minor increased in conductivity post vacuum. This would suggest that placing the samples in a vacuum desorbed them of reducing species

such as CO<sub>2</sub>, similar to what was reported by [18]. The CO<sub>2</sub> acts as an electron trap in the MWCNT composite that reduces the number of available conducting electrons and thus reducing the conductivity of the composite. After 48 hours, the conductivity returned to its original value due to re-absorption of these molecules.

Vacuum effects on EMI-SE were consistent with the increase in conductivity. Sample 4CNT/4GL and sample 2CNT/4CNT/2CNT had roughly a 3 dB increase in EMI-SE. Whereas sample CNT/GLx4 had a 1 dB change in shielding effectiveness. The change in EMI-SE can also be attributed to the removal of air between the layers of the MWCNT composite. The air, having different impedance than the surrounding material, can act as another layer in the composite. Removing the air is like removing an additional layer in the MWCNT composite. This would decrease the multiple reflection component of the overall shielding effectiveness resulting in a higher overall EMI-SE.

**Table 10. Mean EMI-SE Post Electron Irradiation**

	Pre-Irradiation	Post Irradiation	24 Hours	48 Hours	72 Hours	96 Hours
Sample Configuration	Mean EMI-SE (dB)	Mean EMI-SE (dB)	Mean EMI-SE (dB)	Mean EMI-SE (dB)	Mean EMI-SE (dB)	Mean EMI-SE (dB)
8GL	-0.7	-0.7	-0.7	-0.7	-0.7	-0.7
4CNT/4GL	-74.06	-86.04	N/A	N/A	-84.23	-71.61
2CNT/4GL/2CNT	-84.37	-100.58	-99.68	N/A	N/A	-86.29
CNT/GLx4	-71.94	-78.41	-79.40	-78.5	-73.78	-73.27

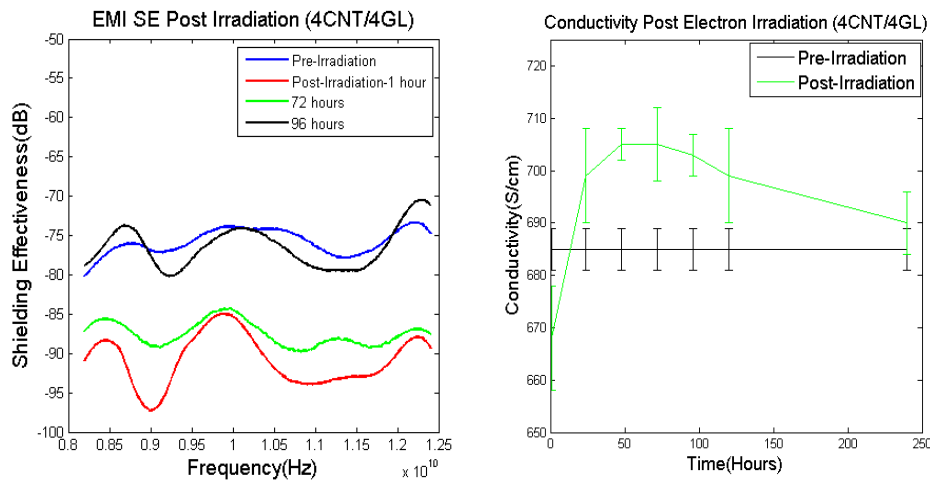
#### 7.4 Electron Irradiation Results

Table 10 contains the average EMI-SE values for all the MWCNT composites post irradiation. Table 11 contains the changes to conductivity of the test material post electron irradiation. Figure 31 thru Figure 34 is a comparison of changes to conductivity

**Table 11. Conductivity Post Electron Irradiation ( $10^{16}$  electrons/cm<sup>2</sup> @ 500 keV)**

Mean Conductivity (S/cm)	4CNT/4G	+/- (S/cm)	2CNT/4G/2CNT	+/- (S/cm)	G/CNTx4	+/- (S/cm)	All-Glass
Pre-Characterization	685	4	453	5	501	27	N/A
Post Irradiation	668	11	439	7	407	15	N/A

and changes to EMI-SE post irradiation. Figure 31 shows an increase in both conductivity and EMI-SE post irradiation in the 4CNT/4GL sample. Also, measurements taken over time showed both EMI-SE and conductivity of the sample returning to pre-irradiation levels. Figure 32 also showed the same trend for the 2CNT/4GL/2CNT. Figure 33 contains the EMI-SE and conductivity measurement of the CNT/GLx4 sample. Unlike the first two samples, the CNT/GLx4 showed a decrease in conductivity post irradiation. In addition, the EMI-SE measurement did not follow the same increasing and then decreasing trend. Figure 34 is a comparison of the four MWCNT composite samples post electron irradiation.

**Figure 31. Changes over time to EMI-SE (left) and conductivity (right) of 4CNT/4GL sample after electron irradiation.**

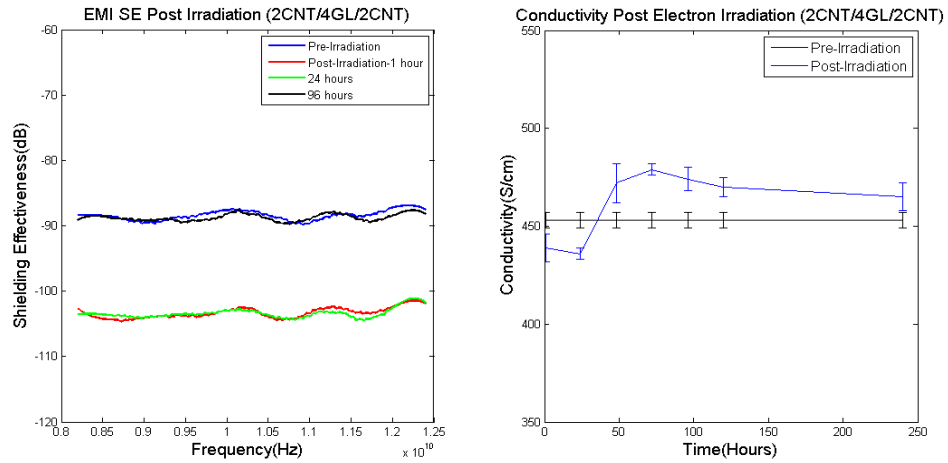


**Figure 33. Changes over time to EMI-SE (left) and conductivity (right) of 2CNT/4GL/2CNT sample after electron irradiation.**

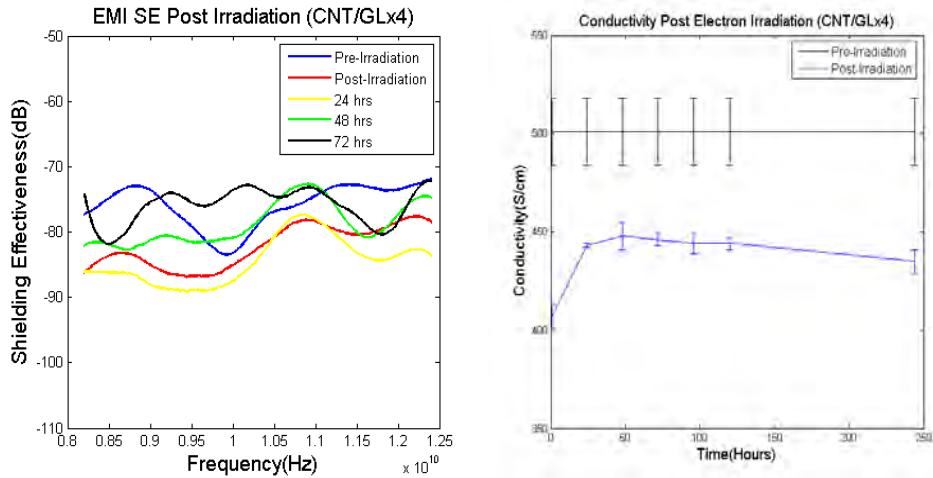


**Figure 32. Changes over time to EMI-SE (left) and conductivity (right) of CNT/GLx4 sample after electron irradiation.**

## 7.5 Electron Irradiation Analysis

As discussed in Chapter IV, CNTs behave drastically different than other materials. Unlike materials such as graphite and amorphous carbon, MWCNT composites conductivity can be enhance when exposed to low level of radiation. Under



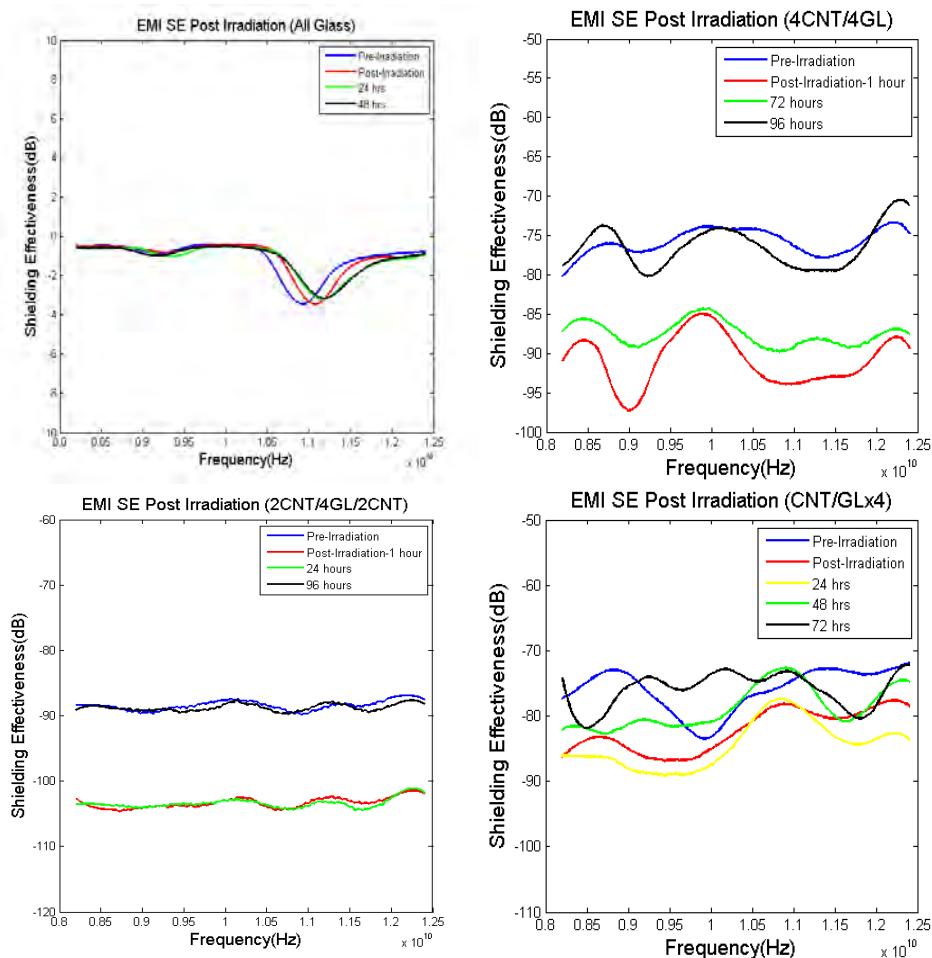


**Figure 34. A comparison of changes to the MWCNT composites post electron irradiation. The four separate figures show the four different sample types as noted in the headings.**

normal conditions, CNTs in bundles interact with one another through the van der Waal forces. The van der Waal force is an attractive force between MWCNTs as a result of temporary fluctuating dipoles. This is a relatively weak force as compared to an ionic or covalent bond. When the CNTs bundles are exposed to electron irradiation with enough energy to displace the carbon atom from its normal lattice position, cross-links can occur. Dangling bonds left behind from the displaced carbon atom can form covalent bonds or cross-links between CNT bundles and between layers of MWCNT. The cross-links

provide additional networks or pathways that allow electrons to travel through the network of MWCNT more easily. The increase in the ability of the electrons to move through the composite increased the conductivity of the MWCNT composites.

Quantitatively, according to Equation IV-1, the additional networks increased the probability of the electrons traveling through the material. The increase in the transmission coefficient ( $T$ ) increased the conductance ( $G$ ) of the material.

In addition to cross-links within the MWCNT, bridging within the epoxy resin and reaction between the epoxy resin and MWCNT can also increase the conductivity of the composite. Reference [47] describes a possible reaction between the CNT and the epoxy resin. As discussed in section 4.4, when the incident particle or photon interacts with the epoxy resin, it generates reactive, transient intermediate free radicals. Radiolytic hydrogen gas from ruptured C-H bonds is formed in the epoxy resin. The radicals formed will interact with one another. In the presence of fillers such as carbon nanotubes, the free radicals will react with the CNT to form permanent covalent bonds. Figure 35 depicts a potential reaction between CNTs and free radicals produced from the scission of the epoxy resin. The pinning of the CNTs to its substrate has also shown an increase in tensile strength of the composite [47] .

It is difficult to determine to what extent the changes to the conductivity can be attributed to cross-links between the polymers in the epoxy resin, reaction between the epoxy resin and MWCNTs or bridging within the MWCNT network. Calculations of maximum energy transfer from the electrons irradiation discussed in section 4.2 and listed in Table 2, demonstrated that the electrons used in the irradiation had enough energy to displace the different atoms of the composite. The hydrogen, nitrogen, oxygen,

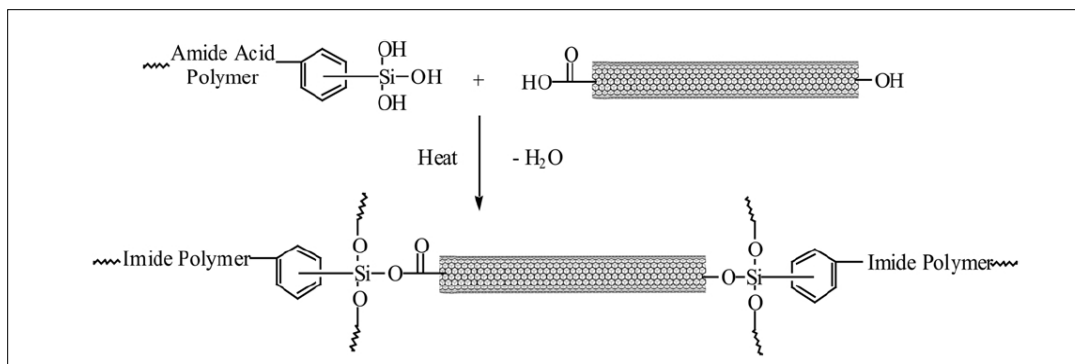


**Figure 35. A potential reaction between CNTs and epoxy resin [47]**

and carbon atoms could all be displaced from their normal lattice position in the MWCNT and epoxy resin. In addition to displacement damage, scission of the polymers in the epoxy resin is also occurring. Long complex polymer chains are broken up into smaller reactive species. These reactive species can then react with the defects in the MWCNT. The pinning of CNT's to its substrate has shown an increase in structural strength in the composite material [47]. As a result of the displacement and scissions, cross-links within the MWCNT, within the epoxy resin and between the MWCNTs and the epoxy resin are all possible and contributing to the increase in conductivity of the composite.

The 4CNT/4GL and 2CNT/4G/2CNT sample had an increase in conductivity post irradiation. The CNT/GLx4 sample; however, had a decrease in conductivity post irradiation. The differences in the behavior of the samples post irradiation suggest that bridging between layers of MWCNT composites also played an important role in the durability of the composite. Irradiation increased the conductivity in the first two samples that had multiple conducting layers side by side. The CNT/GLx4 had four conductive

layers that were separated by the  $\text{SiO}_2$  glass and was not as durable as the first two layered configuration.

Improvement in EMI-SE can be attributed to an increase in conductivity of the material. As discussed in section 5.8, shielding effective is a function of skin depth. The thicker the shield as compared to its skin depth, the better EMI-SE it possesses. Equation V.26 indicates that an increase in conductivity would decrease the skin depth of a material. Equations V.32 and V.33 indicates that decreasing the skin depth while maintaining the same thickness of the material, would increase the overall EMI-SE of the material. Measurements taken after electron irradiation showed an increased in the EMI-SE of the 4CNT/4GL and 2CNT/4GL/2CNT sample. The increase in shielding effectiveness correlates directly with the increase in conductivity of the two samples. However, the CNT/GL $\times$ 4 had an increase in EMI-SE but a decrease in conductivity. There are several possible explanations for the differences. The first explanation is that only the surface conducting layer in the CNT/GL $\times$ 4 had a decrease in conductivity. Whereas the remaining conductive layers embedded in the sample experienced an increase in conductivity. The second explanation is the electron irradiation could have sintered the layers of the CNT/GL $\times$ 4 which could also increase the EMI-SE independent of the decrease in conductivity of the material. As discussed in the previous section, the initial EMI-SE of the CNT/GL $\times$ 4 was lower than the other two samples. It is possible that the difference in the measured values was due to air gaps in the CNT/GL $\times$ 4 that could act as additional layers and decrease the overall EMI-SE. The sintering during the irradiation heated and fused the layers together, decreasing the multiple reflections within

the sample and mitigated the interface effects that initially reduced the overall EMI-SE of the CNT/GL×4 sample.

**Table 12. Mean EMI-SE Post Neutron Irradiation**

	Pre-Irradiation		Post Neutron(1)	Post Neutron(2)	96 Hours	168 Hours
Sample Configuration	Mean EMI-SE(dB)	± (dB)	Mean EMI-SE (dB)	Mean EMI-SE (dB)	Mean EMI-SE (dB)	Mean EMI-SE (dB)
8GL	-0.7	0.3	-0.8	-0.7	-0.7	-0.7
4CNT/4GL	-75.30	0.02	-76.14	-76.14	-76.14	-77.62
2CNT/4GL/2CNT	-85.59	.01	-85.59	-86.05	-86.05	-86.05
CNT/GL×4	-73.93	.02	-73.93	-74.60	-74.60	-76.87

## 7.6 Neutron Irradiation results

The MWCNT were irradiated with 1.0 MeV Si(eq) neutrons from the OSURR to a fluence level of  $10^{14}$  neutrons/cm<sup>2</sup> and  $10^{15}$  neutrons/cm<sup>2</sup>. Table 12 gives the mean EMI-SE for the MWCNT composites post neutron irradiation. Table 13 gives the conductivity results for the MWCNT composites. Figure 37 thru Figure 38 are graphical representations of the data. The graphs showed that neutron irradiation had no

**Table 13. Conductivity results Post Neutron Irradiation**

Mean Conductivity (S/cm)	4CNT/4G	+/- (S/cm)	2CNT/4G/2CNT	+/- (S/cm)	G/CNT×4	+/- (S/cm)	All-Glass
Pre-Characterization	766	13	388	10	458	26	N/A
Post Irradiation $1 \times 10^{14}$ neutrons/cm <sup>2</sup>	754	10	399	7	469	6	N/A
Post Irradiation $1 \times 10^{15}$ neutrons/cm <sup>2</sup>	743	11	402	3	457	7	N/A

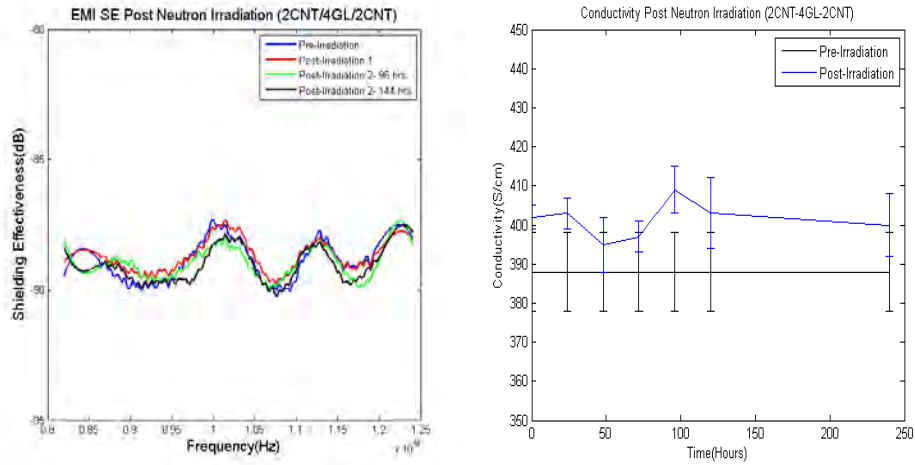


**Figure 37. Changes over time to EMI-SE (left) and conductivity (right) of 2CNT/4GL/2CNT sample after neutron irradiation.**

measurable effects on the MWCNT composites. The changes to conductivity and EMI-SE were within the standard deviation of the pre-irradiation measurement. The results are consistent with [29] and [30] which reported that carbon nanotube composites would experience little or no change in conductivity with fluence lower than  $10^{16}$  ions/cm<sup>2</sup>.

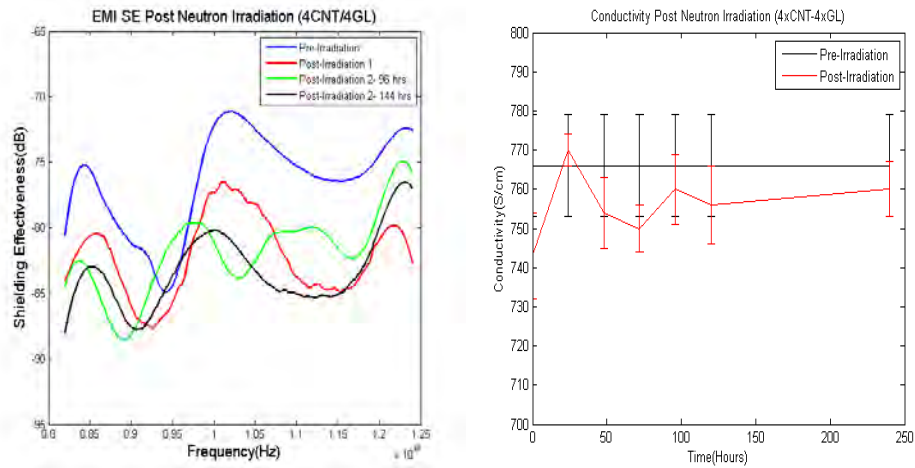


**Figure 36. Changes over time to EMI-SE (left) and conductivity (right) of 4CNT/4GL sample after neutron irradiation.**

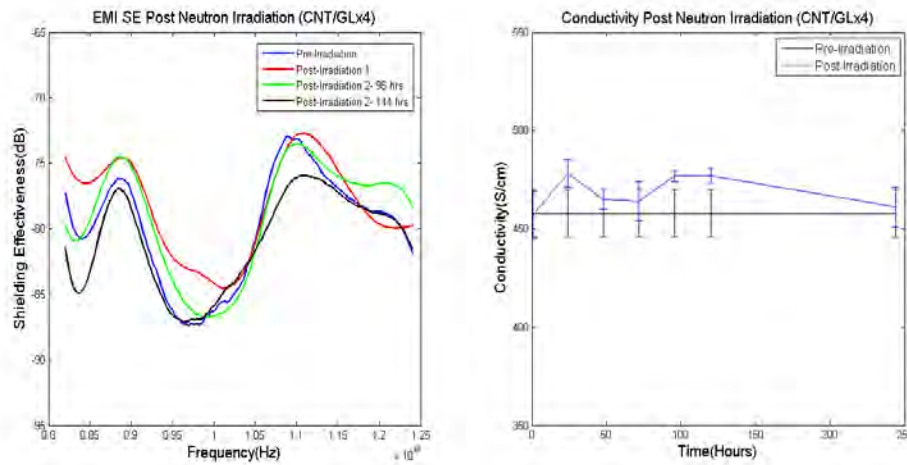


**Figure 38. Changes over time to EMI-SE (left) and conductivity (right) of CNT/GLx4 sample after neutron irradiation.**

## 7.7 Error Analysis

An analysis of variance (ANOVA) was conducted on the pre-characterize conductivity data collected on the MWCNT composites. The one-way ANOVA, which treats each sample type as a separate group indicated that the group mean are not the same. Sample 4CNT/4GL had a higher conductivity than the other two samples. This indicates that the different conductive layers of the 4CNT/4GL samples are interacting with one another. As discuss in section 4.3, additional charge carrier transport pathways can increase the conductance of the material. Bridging between the four layers of MWCNT composite provided additional pathways that increased the overall conductance of the 4CNT/4GL sample. Figure 39 is the box-plot from the one-way ANOVA. On each box, the central read line represents the median and the edges of the box are the 25<sup>th</sup> and 75<sup>th</sup> percentiles. The distances between the tops and bottoms are the interquartile ranges. The whiskers extend to the most extreme data points not considered outliers and outliers

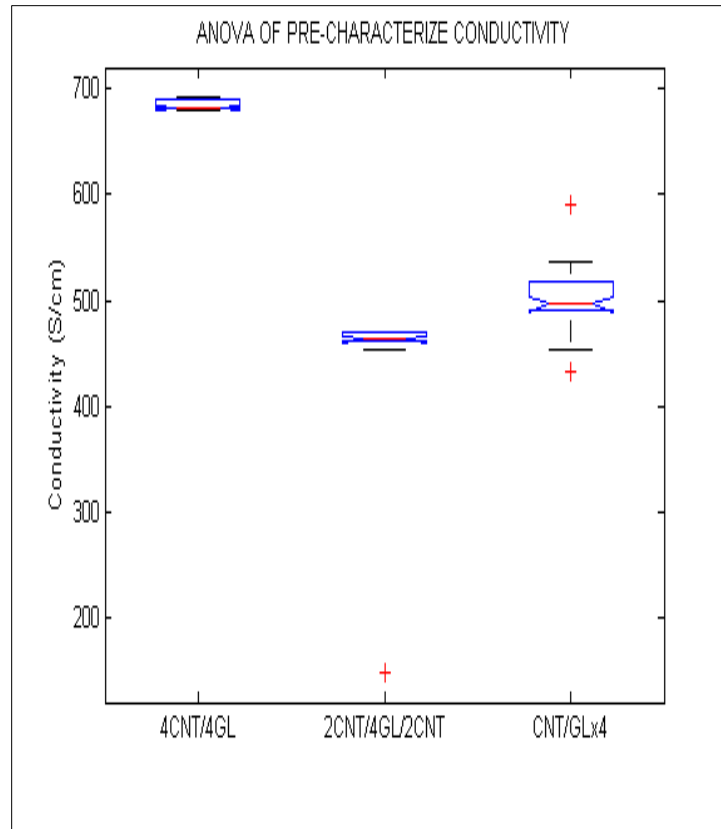


**Figure 39. Analysis of variance between pre-characterized conductivity of different sample types.**

are plotted individually as red plus signs. Outliers are data that are 1.5 times the interquartile range away from the top or bottom of the box [46] .

A one way ANOVA test was also conducted on the individual MWCNT composites post vacuum and post electron irradiation. Figure 40 shows the result from the one way ANOVA test. All three samples show an initial decrease in conductivity post vacuum and post electron irradiation. The notches next to the red line in each of the sample show the variability of the median between samples. The width of a notch is computed so that box plots whose notches do not overlap have different medians at the 5 % significance level. The significance level is based on a normal distribution



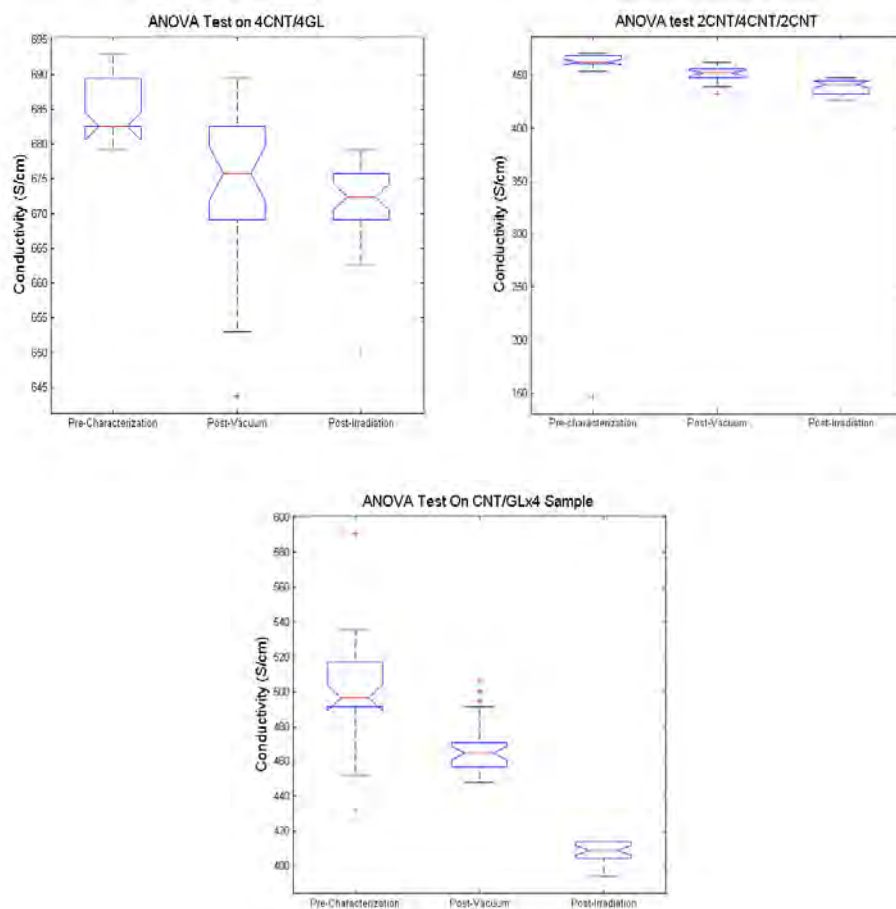


**Figure 40. Analysis of variance between pre-characterized, post vacuum and post irradiation conductivity of the different sample types. The three separate figures show the three different sample types as noted in the headings.**

assumption. If the notches in the box plot do not overlap, there is a 95% chance that the true median is different. For the 4CNT/4GL sample, the notches on the box plot of the post vacuum and post irradiation overlapped. The overlapping notches indicate that the probability of the median changing is less than 95%. . Both the 2CNT/4GL/2CNT and the CNT/GL $\times$ 4 have a 95% probability that the conductivity decreased post vacuum and post electron irradiation. In addition, Figure 41 also shows that the median was not centered on the box plot. This indicates that the data collected was skewed.

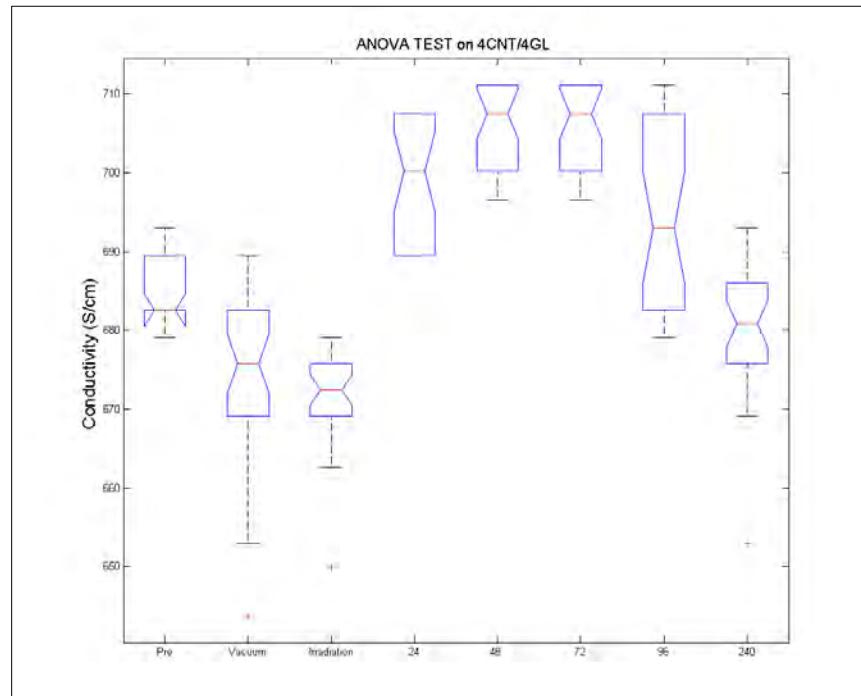


**Figure 41. Analysis of variance of the 4CNT/4GL sample**

## VIII. Conclusion and Recommendation

The purpose of this research was to characterize electrical properties of carbon nanotube containing composites intended for use as satellite surface materials before and following electron and neutron irradiation. The MWCNT composites were irradiated with electrons to fluence levels of  $10^{16}$  electrons/cm<sup>2</sup> with 500 keV electrons. In addition, 1.0 MeV Si (eq) neutrons was used to irradiate all the composites to a fluence of  $10^{14}$  neutrons/cm<sup>2</sup> and  $10^{15}$  neutrons/cm<sup>2</sup>. Results show that the changes to the MWCNT composites' electrical properties were insignificant. The multi-walled carbon nanotube composites exhibited high conductivity and high EMI-SE that is consistent with conductive materials and were highly durable under the simulated space radiation environment.

A secondary purpose of the research was to investigate which layered configuration was the most durable under electron and neutron irradiation. Although the differences were minor, the 2CNT/4GL/2CNT and the 4CNT/4GL configuration were most durable under electron irradiation. The 2CNT/4GL/2CNT configuration consistently had the best EMI-SE while the 4CNT/4GL had the higher conductivity. In addition, both samples had an increase in conductivity and EMI-SE post electron irradiation. The CNT/GL×4 sample had a decrease in conductivity and an increase in EMI-SE post electron irradiation. This would suggest that the different layered configuration does play a role in the durability of the composite. Having multiple conductive layers of MWCNT composites provide increased durability against electron irradiation. Additionally, the differences also indicate that conductivity is not the only mechanism affecting the EMI-SE of the composite. Irradiation was conducted on three

2CNT/4GL/2CNT panels to a fluence of  $10^{16}$  electrons/cm<sup>2</sup> with 100, 200 and 500 keV electrons to investigate the possibility of ionizing radiation effects on the panels.

However, no changes in the EMI-SE were observed for these irradiations. Overall, the changes to the electrical properties of the samples were minor, and results from follow on electron were inconclusive. Further investigations are required to determine whether the effects of the electron irradiation are due to transient ionizing effects or to displacement damage.

The effects of neutron radiation on the electrical properties of the MWCNT composites were also inconclusive. Neutron radiation is more damaging than electron radiation. However, the MWCNT composites did not experienced the same changes to its electrical property post neutron irradiation as it did post electron irradiation. This could suggest that the changes observed post electron irradiation was due to ionizing effects and not due to displacement damage. However, another possible explanation is that the neutron irradiation did not create the same number of defects in the MWCNT composites as the electron irradiation. The neutron spectrum of the OSURR was converted to a 1 MeV equivalent. The conversion factor used was for silicon instead of CNTs which could have introduced significant error in the calculation. The crystalline structure of silicon is denser than the open structure of the MWCNTs. As a result, a much higher fluence is required to create the same damage in the MWCNTs. In order to measure the same changes observed post electron irradiation, the MWCNT composites needed to be irradiated to higher neutron fluence.

Changes to the electrical properties of the MWCNT composites post vacuum were also inconsequential. However, there was a measurable decrease in the conductivity

of the composites that merits consideration in future research. In addition, recovery of the composites' conductivity over time post irradiation can also be attributed to the re-absorption of reducing gas such as CO<sub>2</sub>. Future research should attempt to measure the conductivity of the material in situ. This will determine whether the recovery of the composites' conductivity to its original level was due to re-absorption of gases in the atmosphere.

As highlighted by [1] and [3], the HDPE setup used to measure the samples needed to be modified in order to decrease measurement variations. However, it is recommended that the entire resistivity measurement using the HDPE fixture be replaced by another method. The current method is an unnecessary waste of time and resources. The method required separate samples to be cut in order to fit the HDPE fixture. The resistivity measurements and EMI-SE measurements required samples that were different sizes. As a result, two separate sets of MWCNT composites were required to conduct the same experiment. The composites are non-homogenous. Having two sets of samples made it difficult to correlate the results from the EMI-SE and the conductivity measurements. The van der Pauw measurement technique is highly recommended for future investigation. The same size sample can be used for both the van der Pauw resistivity measurement and the EMI-SE. Also, the variation caused by the placement of the sample while using the HDPE would also be reduced.

The MWCNT composite have shown the ability to retain its electrical properties following a simulated space radiation environment. The composite can be an excellent choice for applications that require high conductivity and radiation resistance. However, the results of the research highlighted the need for additional investigation in order to

develop a better understanding of the fundamental causes to the changes that took place following irradiation.

## Appendix A

**Table 14: Network Analyzer calibration steps**

1	Select: Network Analyzer software application
2	Select: File, Recall previous test
3	Set Begin and End frequencies: Yellow = 8.2 GHz; Green = 12.4 GHz
4	Select: Calibration Wizard
5	Select: Unguided, TRL, 1-2 Ports, Cal Kit #28 (X-band)
6	Select: Next, Through Standard, Reflect Standard
7	Insert SHORT plate onto adapter (piece without rectangular hole)
8	Select: both SHORT push-buttons
9	Remove SHORT plate
10	Insert LINE plate onto adapter (thickest piece with rectangular hole)
11	Select: LINE push-button, X-Band $\frac{1}{4}$ wavelength line, Next
12	Remove LINE plate
13	Tighten both end adapters with nothing in between
14	Select: THRU, Next, Finish

## Bibliography

- [1] Duncan, Nickolas A. *Changes to Electrical Conductivity In Irradiated Carbon Nanocomposites*. MS Thesis, AFIT/GNE/ENP/11-M06, Air Force Institute of Technology(AU), Wright-Patterson AFB-OH, 2011.
- [2] Chong, Kenneth Y. *Evaluation of Nanocomposites for Shielding Electromagnetic Interference*. MS Thesis, AFIT/GAE/ENY/11-S01, Air Force Institute of Technology(AU), Wright-Patterson AFB-OH, 2011.
- [3] Coy, David, F. *Changes To Electrical Conductivity in Irradiated Carbon-Nickel Nanocomposites*. MS Thesis, AFIT/GNE/ENP/10-M02, Air Force Institute of Technology(AU), Wright-Patterson AFB OH, 2010.
- [4] MIL-STD-1809, United States Air Force, “*Space Environment for USAF Space Vehicles*,” February 15, 1991, pp. 20-23.
- [5] [Van Allen belt]. Retrieved December 12, 2011, from:  
<http://www.ati.ac.at/~vanaweb/spacerad.html>
- [6] Paul, Clayton R. *Introduction to Electromagnetic Compatibility*. New York: John Wiley & Sons, INC.
- [7] Iijima, Sumio "Helical microtubules of graphitic carbon," *Nature*,354, 56-58 (November 1991).
- [8] Mall, Shankar. “Carbon Nanotube Bucky Paper” Electronic Message. 15 November 2010.
- [9] [Single wall and multi-wall carbon nanotues] Retrieved December 12, 2011, from  
[http://www-ibmc.u-strasbg.fr/ict/vectorisation/nanotubes\\_eng.shtml](http://www-ibmc.u-strasbg.fr/ict/vectorisation/nanotubes_eng.shtml)
- [10] O’Connell, Michael “Carbon Nanotubes Properties and Applications”, Florida: CRC Press, 2006.
- [11] Ruoff, Rodney S., Qian, Dong and Liu, Wing K. Mechanical properties of carbon nanotubes: theoretical predictions and experimental measurements 2003.
- [12] McEuen, Paul L., Park, Ji-Yong. "Electron Transport in Single-Walled Carbon Nanotubes." Retrieved February 28, 2012, form  
<http://www.mrs.org/publication/bulletin>



- [13] Fouracre, R. A., Al-Attabi, A., Banford, H. M., Given, M. J. and Tedford, D. J. Radiation effects in epoxy resin system: gamma rays, neutrons and high energy electrons 1990.
- [14] Khare, Rupush and Bos, Suryasarathi. "Carbon Nanotube Based Composites –A Review," *Journal of Minerals & Materials Characterization & Engineering*, 4(1):31-46 (2005).
- [15] Weber, Mark, and Musa R. Kamal. 1997. Estimation of the volume resistivity of electrically conductive composites. *Polymer Composites* 18 (6): 711-25.
- [16] Kim, Ki Hong, and Won Ho Jo. 2009. "A strategy for enhancement of mechanical and electrical properties of polycarbonate/multi-walled carbon nanotube composites." *Carbon* 47 (4) (4): 1126-34.
- [17] Maeda, Shusaku and others. "Change in carbon nanofiber resistance from ambient to vacuum," *AIP Advances*, 1, 022102 14 April 2011  
[http://aipadvances.aip.org/resource/1/aaidbi/v1/i2/p022102\\_s1?view=fulltext&bypassSSO=1](http://aipadvances.aip.org/resource/1/aaidbi/v1/i2/p022102_s1?view=fulltext&bypassSSO=1)
- [18] Jijun Zhao and Alper Buldum and Jie Han and Jian,Ping Lu. "Gas molecule adsorption in carbon nanotubes and nanotube bundles." *Nanotechnology* 13 (2002)  
[http://scholar.google.com/scholar?q=Gas+molecule+adsorption+in+carbon+nanotube+s+and+nanotube+bundles&hl=en&as\\_sdt=0&as\\_vis=1&oi=scholar](http://scholar.google.com/scholar?q=Gas+molecule+adsorption+in+carbon+nanotube+s+and+nanotube+bundles&hl=en&as_sdt=0&as_vis=1&oi=scholar)
- [19] Zahab, A. et. al. "Water-vapor effect on the electrical conductivity of a single-walled carbon nanotube mat," *Phys. Rev. B*, 62 October 2000.  
<http://link.aps.org/doi/10.1103/PhysRevB.62.10000>
- [20] Keat Ghee Ong, Kefeng Zeng, & Grimes, C. A. (2002). A wireless, passive carbon nanotube-based gas sensor. *Sensors Journal*, IEEE, 2(2), 82-88.
- [21] Petrosky, James. Class handout, NENG 660, "Radiation Effects on Electronic Devices," Department of Engineering Physics, Air Force Institute of Technology, Wright-Patterson AFB OH, Summer 2010.
- [22] McClory, John W. *The Effect of Radiation on the Electrical Properties of Aluminum Gallium Nitride/Gallium Nitride Heterostructures*. Dissertation, AFIT/DS/ENP/08-01, Air Force Institute of Technology (AU), Wright-Patterson AFB-OH, 2011.
- [23] F. Banhart. "Irradiation of carbon nanotubes with a focused electron beam in the electron microscope." *Journal of Materials Science*. Vol 41 Number 14 July 2006.

- [24] A. V. Krasheninnikov et al. "Stability of carbon nanotubes under electron irradiation: Role of tube diameter and chirality." *PHYSICAL REVIEW B* 72, 125428 2005.
- [25] Suzuki, S., Yamaya, K., Homma, Y., & Kobayashi, Y. (2010). Activation energy of healing of low-energy irradiation-induced defects in single-wall carbon nanotubes. *Carbon*, 48(11), 3211-3217.
- [26] Tatro, S. R., Clayton, L. M., O'Rourke Muisener, P. A., Rao, A. M., & Harmon, J. P. (2004). Probing multi-walled nanotube/poly(methyl methacrylate) composites with ionizing radiation. *Polymer*, 45(6), 1971-1979.
- [27] Holmes-Siedle, Andrew and Adams, Len. *Handbook of Radiation Effects*, New York: Oxford University Press, 2002.
- [28] Fouracre, R. A., Al-Attabi, A., Banford, H. M., Given, M. J., & Tedford, D. J. (1990). Radiation effects in epoxy resin system: Gamma rays, neutrons and high energy electrons. Paper presented at the *Electrical Insulation and Dielectric Phenomena*, 1990. Annual Report, Conference on, pp. 114-119.
- [29] Krasheninnikov, A V. and Nordlund, K. "Irradiation effects in carbon nanotubes." *Nuclear Instruments and Methods in Physics Research Section B: Beam Interactions with Materials and Atoms*. 2004.
- [30] Krasheninnikov, A V. and Nordlund, K. "Formation of ion-irradiation-induced atomic-scale defects on walls of carbon nanotubes." *Physical Review B*, Volume 63, May 2001.
- [31] Smith, Brian W. and Luzzi, David E. "Electron irradiation effects in single wall carbon nanotubes." *Journal of applied Physics*. Vol. 90 Number 7, 1 October 2001.
- [32] Basiuk, Vladimir and Basiuk, Elena. *Chemistry of Carbon Nanotubes*, California: American Scientific Publishers, 2008.
- [33] Valdes, L., Resistivity Measurements on Germanium for Transistors, Proc. I.R.E, 42, Feb., 1954, p.420.
- [34] Uhler, A., Jr., The Potentials of Infinite Systems of Sources and Numerical Solutions of Problems in Semiconductor Engineering, B.S.T.J, 34, Jan., 1955, p. 105
- [35] Smits, F. M. Measurement of Sheet Resistivities with the Four-Point Probe, B.S.T.J, 1957.

- [36] Chase, Gene. "Ohms Per Square What!" *ESD Journal*, 2011.  
<http://www.esdjournal.com/techpaper/ohms.htm>
- [37] Griffiths, D. J. (1998). *Introduction to Electrodynamics* (3rd Edition). Benjamin Cummings
- [38] Tupta, Mary, A. "Techniques for Measuring the Electrical Resistivity of Bulk Materials." Keithley Instruments, Inc. Lecture given over Internet. 2010.
- [39] Keithley Instruments, Inc. *Low Level Measurement Handbook. Precision DC Current, Voltage, and Resistance Measurements*. 6<sup>th</sup> Edition, 2004.  
[http://www.keithley.com/knowledgecenter/knowledgecenter\\_pdf](http://www.keithley.com/knowledgecenter/knowledgecenter_pdf)
- [40] Hochberg and Phil Foster. "Four Point Probe I-V Electrical Measurements using the the Zyvex Test System Employing a Keithley 4200," 2006.  
<http://www.dcgsystems.com/>
- [41] Knott, Eugene F, Shaeffer John F. and Tuley, Michael T. *Radar Cross Section*. Second Edition, Massachusetts: Artech house, INC.
- [42] The Ohio State University Research Reactor website <http://reactor.osu.edu/pictures>
- [43] ASTM E722-94, "Standard Practice for Characterizing Neutron Energy Fluence Spectra in Terms of an Equivalent Monoenergetic Neutron Fluence for Radiation-Hardness Testing of Electronics," ASTM international, 1994.
- [44] Beuneu, F, C. l'Huillier, J.P. Salvetat, J.M.Bonard, and L. Forro. "Modification of multiwall carbon nanotubes by electron irradiation: An ESR study," *Physical Review*, Volume 59, Number 8, February 1999.
- [45] Kaufmann, Andrew. "7 Inch Dry Tube." Electronic message with excel spreadsheet and word attachment.
- [46] MATLAB version R2011a. Natick, Massachusetts: The MathWorks Inc., 2012.
- [47] Smith, J.G. et. Al. "Space durable polymer/carbon nanotubes films for electrostatic charge mitigation." *Polymer*, 45 2004.

<b>REPORT DOCUMENTATION PAGE</b>				Form Approved OMB No. 074-0188	
<p>The public reporting burden for this collection of information is estimated to average 1 hour per response, including the time for reviewing instructions, searching existing data sources, gathering and maintaining the data needed, and completing and reviewing the collection of information. Send comments regarding this burden estimate or any other aspect of the collection of information, including suggestions for reducing this burden to Department of Defense, Washington Headquarters Services, Directorate for Information Operations and Reports (0704-0188), 1215 Jefferson Davis Highway, Suite 1204, Arlington, VA 22202-4302. Respondents should be aware that notwithstanding any other provision of law, no person shall be subject to a penalty for failing to comply with a collection of information if it does not display a currently valid OMB control number.</p> <p><b>PLEASE DO NOT RETURN YOUR FORM TO THE ABOVE ADDRESS.</b></p>					
1. REPORT DATE (DD-MM-YYYY) 22-03-2012		2. REPORT TYPE Master's Thesis		3. DATES COVERED (From – To) June 2010 – March 2012	
TITLE AND SUBTITLE  Durability of MWCNT Composites under Electron and Neutron Irradiation				5a. CONTRACT NUMBER	
				5b. GRANT NUMBER	
				5c. PROGRAM ELEMENT NUMBER	
6. AUTHOR(S)  Lu, Quan-Hai T., Major, USA				5d. PROJECT NUMBER If funded, enter ENR #	
				5e. TASK NUMBER	
				5f. WORK UNIT NUMBER	
7. PERFORMING ORGANIZATION NAMES(S) AND ADDRESS(S) Air Force Institute of Technology Graduate School of Engineering and Management (AFIT/EN) 2950 Hobson Way, Building 640 WPAFB OH 45433-7765				8. PERFORMING ORGANIZATION REPORT NUMBER  AFIT/NUCL/ENP/12-M05	
9. SPONSORING/MONITORING AGENCY NAME(S) AND ADDRESS(ES) Air Force Research Laboratory Max D. Alexander 2941 Hobson Way Wright Patterson, OH 45433-7750 (937)785-9135 max.alexander@wpafb.af.mil				10. SPONSOR/MONITOR'S ACRONYM(S) USAF AFMC AFRL	
				11. SPONSOR/MONITOR'S REPORT NUMBER(S)	
12. DISTRIBUTION/AVAILABILITY STATEMENT APPROVED FOR PUBLIC RELEASE; DISTRIBUTION UNLIMITED.					
13. SUPPLEMENTARY NOTES					
14. ABSTRACT <p>Electromagnetic interference shielding effectiveness and conductive properties of carbon nanotube containing composites intended for use as satellite surface materials have been investigated following electron and neutron irradiation. The MWCNT composites were irradiated to fluence levels of <math>10^{16}</math> electrons/cm<sup>2</sup> with 500 keV electrons. Increase in EMI-SE and conductivity was observed following electron irradiation in two of the samples. The sample with alternating layers of MWCNT and glass had a decrease in conductivity and an increase in EMI-SE post irradiation. This would suggest that the different layered configuration does play a role in the durability of the composite. Having multiple conductive layers of MWCNT composites provide increased durability against electron irradiation. Additional electron irradiations were conducted on three MWCNT composite with the two layers of MWCNT on the outside and 4 layers of glass sandwich in the center. The second set of MWCNT composites were irradiated with 1.0 MeV Si(eq) neutrons to a fluence level of <math>10^{14}</math> neutrons/cm<sup>2</sup> and <math>10^{15}</math> neutrons/cm<sup>2</sup>. Minor changes in the conductivity and no change in EMI-SE was observed in the MWCNT composites. The overall changes observed; however, are inconsequential to MWCNT composites' intended use as satellite surface structure. In addition, the different layered configurations did have an effect on the electrical properties and durability of the composite under irradiation. The sample with the alternating layer of MWCNT and glass had the least favorable configuration of the three designs.</p>					
15. SUBJECT TERMS Conductive composites, radiation effects					
16. SECURITY CLASSIFICATION OF:			17. LIMITATION OF OF ABSTRACT  UU	18. NUMBER OF PAGES  108	19a. NAME OF RESPONSIBLE PERSON LTC John, McClory AFIT/ENP
a. REPORT  U	b. ABSTRACT  U	c. THIS PAGE  U			19b. TELEPHONE NUMBER (Include area code) (937) 255-6565, ext 7308 (john.mcclory@afit.edu)